Graduate Theses, Dissertations, and Problem Reports

2023

Optimal Design and Operation of Integrated Hydrogen Generation and Utilization Plants

Ijiwole Solomon Ijiyinka
West Virginia University, isi00001@mix.wvu.edu

Optimal Design and Operation of Integrated Hydrogen Generation and Utilization Plants

Ijiwole Solomon Ijiyinka

Thesis submitted to the

Benjamin M. Statler College of Engineering and Mineral Resources

at West Virginia University

in partial fulfillment of the requirements

for the degree of

Master of Science

In

Chemical Engineering

Debangsu Bhattacharyya, Ph.D., Chair

Yuhe Tian, Ph.D.

Oishi Sanyal, Ph.D.

Department of Chemical and Biomedical Engineering

Morgantown, West Virginia

2023

ABSTRACT

Optimal Design and Operation of Integrated Hydrogen Generation and Utilization Plants

Ijiwole Solomon Ijiyinka

There are considerable efforts worldwide for reducing the use of fossil fuel for energy production. While renewable energy sources are being increasingly used, fossil fuel still contribute about 80% of the energy used worldwide. As a result, the level of CO_2 is still increasing fast in the atmosphere currently exceeding about 410 parts per million (ppm). For reducing CO_2 build up in the atmosphere, various approaches are being investigated. For the electric power generation sector, two key approaches are post-combustion CO_2 capture and use of hydrogen as a fuel for power generation. These two solutions can also be integrated together in a flexible power plant configuration.

This research presents two novel energy systems where hydrogen is being utilized in a power plant for the co-firing of natural gas. The first system is NGCC power plant integrated with a post combustion carbon capture technology and hydrogen production unit. The second system is a standalone Peaker plant (simple cycle plant) integrated with hydrogen production unit. The techno-economic analysis of these two systems will enable us to understand the optimal design and operational performance of this energy systems.

The Net Present Value (NPV) optimization was used for the techno-economic analysis of the two energy systems at different conditions. Different tax scenario was also investigated for the electricity price (LMP) used in the optimization scheme. As part of development of optimization work, reduced order models (ROM) were developed for the more sophisticated and nonlinear models of the standalone models. A clustering algorithm with a derivative consideration was also developed to reduce the number of optimization days needed for a year-long optimization. For these two-hydrogen utilization configuration, the optimal design conditions of the hydrogen production unit were decided, and it was shown that these optimal values change with the electricity market profiles.

Dedication

I dedicate this thesis to Almighty God and my late parents Mr. Julius Eniola Ijiyinka and Mrs. Omonike Omolara Ijiyinka

Acknowledgement

I would like to thank God almighty for his unflinching love and unlimited support for me in the course of my career so far. I would also like to appreciate the effort of my late parent Mr & Mrs Julius Ijiyinka for putting me on the path of education. In the same light, I also appreciate the support and love I got from my wife, Damilola my sisters, Jumoke and Yetunde and my friend, Temitope during this program.

It's imperative for me to appreciate my advisor, Dr. Debangsu Bhattacharyya for his mentorship, expertise and support during the course of my program. His acceptance of me into his research group means a lot to me and the opportunity he gave me to learn will always be special to me. Also, my sincere appreciation goes to my Advisory and Examining Committee members, Dr. Yuhe Tian and Oishi Sanyal

I would like to extend my heartfelt gratitude to members of the Advanced Process and Energy Systems Engineering Group for their cooperation and collaborations in the course of my research. I'm particularly grateful to our associate research professor, Dr. Emdad Haque and my colleague Stephen.

Table of Contents

List Of Figures

List Of Tables

Chapter 1

Introduction

There are considerable efforts worldwide for reducing the use of fossil fuel for energy production [1]. While renewable energy sources are being increasingly used, fossil fuel still contribute about 80% of the energy used worldwide [2]. As a result, the level of CO_2 is still increasing fast in the atmosphere currently exceeding about 410 ppm [3]. For reducing CO_2 build up in the atmosphere, various approaches are being investigated. For the electric power generation sector, two key approaches are post-combustion CO_2 capture and use of H_2 as a fuel for power generation.

Various post-combustion capture technologies are being investigated that can provide 90% and above CO_2 capture rate [4]. It is anticipated that future capture plants will be operating flexibly where their capture rates and load can considerably vary with time. Irrespective of the capture technology, these flexible capture plants should be optimally designed and operated for maximizing their profit and minimizing environmental footprints of CO_2.

Another strategy is utilization of hydrogen as a fuel in power plants that can reduce CO_2 emission by over 30-40% [5]. Hydrogen can be used as an energy storage medium producing it during the time of low demand and abundant availability of renewable-based power while utilizing it later when demand is high and/or availability of renewable-based power is not sufficient to satisfy the demand. H_2 can be stored in different ways- as a liquid under cryogenic condition, as a pressurized gas, and in the form of solid or liquid hydrides [6]. Out of these, storing of compressed gas is currently the cheapest and most practical option especially for distributed storage. However, capacity and maximum operating pressure of storage must be optimal for cost-efficient storage of hydrogen [7,8]. There are three leading approaches for utilization of stored H_2 for power generation-co-injection with natural gas in an existing natural gas combined cycle (NGCC) power plant, firing of H_2 by itself in a turbine, and use it in a fuel cell. Co-injection of H_2 with natural gas facilitates use of existing gas turbines in NGCC plants and existing infrastructure. While many existing gas turbine frames have the capability of using reasonably large percentage of H_2 without considerable upgrade, firing of pure H_2 can be challenging in existing frames without considerable upgrade of H_2 as well as modification of the heat recovery steam generator (HRSG). When H_2 is fired by itself, it can be used under simple cycle or combined cycle modes. One of the

early adapters for utilization of pure H_2 is expected to be the Peaker plants that operate under simple cycle mode. In this research, H_2 injection in an existing NGCC plant and firing of H_2 in a Peaker plant will be considered.

1.1 Background and Literature Review

1.1.1 Hydrogen as a Fuel

Energy density of H_2 on mass basis is about 3 times more than the traditional fossil fuels as seen in Table 1 [6]. However, one major challenge is the low volumetric energy density of H_2. While storing H_2 as a liquid can improve its volumetric energy density, cryogenic conditions are needed for liquefaction of H_2 adding to cost. Cost-effective storage of H_2 in form of liquid and solid hydrides still requires considerable research. Storage of H_2 as a compressed gas is one of the viable and matured options.

Table 1. Gravimetric and Volumetric Energy Density for Some Common Fuels [6]

Fuel	Gravimetric Energy Density (MJ/kg)	Volumetric Energy Density (MJ/L)
Hydrogen (Liquid)	143	10.1
Hydrogen (compressed,700bar)	143	5.6
Hydrogen (ambient Pressure)	143	0.0107
Methane (ambient pressure)	55.6	0.0378
Natural Gas (Liquid)	53.6	22.2
Natural Gas (Compressed,250bar)	53.6	9
Natural Gas (ambient pressure)	53.6	0.0364
LPG propane	49.6	25.3
LPG butane	49.1	27.7
Gasoline (Petrol)	46.4	34.2
Biodiesel oil	42.2	33
Diesel	45.4	34.6
Kerosene	46.4	36.7

Flash point of hydrogen is also the lowest (-231°C) when compared to that of other common fuels [9]. For example, methane and biodiesel have flash points of -188°C and 130°C, respectively. The very low flash point of hydrogen makes it easy for imitating ignition and

continuing it. Furthermore, hydrogen has a flammability range of 4-75%, making it the most flammable of the common fuels compared in [6]. While these characteristics make H_2 easy to combust, they also lead to safety concern and therefore additional considerations are needed for designing the combustors for handling pure H_2.

1.1.2 Hydrogen Generation

Fossil fuels are still the major sources of hydrogen globally today with only a very low amount of Hydrogen being produced globally from water electrolysis [10]. Hydrogen production through the electrolysis of water by using renewable energy sources is a focus in many papers [11,12,13,14]. Alkaline electrolyzers, proton exchange membrane (PEM) electrolyzers and solid oxide electrolyzers are the three known types of water electrolyzers. Kewei et.al.[15] developed multiphysics models to compare the three types of electrolyzers. Some of the key operating parameters are presented in Table 2. While power-to-hydrogen efficiency and energy conversion efficiency of solid oxide electrolyzer are the highest, this technology is comparatively less mature and commercial compared to alkaline and PEM electrolyzers. Furthermore, solid oxide electrolyzers operate at a temperature of about 700-1000ºC making it challenging to maintain these the temperature especially for distributed applications.

Table 2. Operational condition of AE, PEM and SO Electrolyzer [15]

	Alkaline Electrolyser	PEM Electrolyser	Solid Oxide Electrolyser
Current density A/cm^2	0.25-0.45	1.0-2.0	0.3-1.0
Cell voltage (V)	1.8-2.5	1.8-2.2	0.9-1.2
Operating pressure (bar)	10-30	20-50	1.0-15
Lower Partial load range (%)	20-40	0-10	-
Power-to-hydrogen efficiency (%)	50-60	65-70	90-96
Energy conversion efficiency (%)	50-65	65-75	75-81
Operating temperature (ºC)	60-90	50-80	700-1000

Figure 1 shows efficiencies at different current density (i.e., at different H_2 production rates) for the three types of electrolyzers [15]. Figure 1 shows that PEM electrolyzers has higher efficiency than alkaline electrolyzers at the same current density. Other competitive advantages of PEM electrolyzers include high voltage efficiency, rapid system response, high gas purity and

compact system design. However, the cost of PEM technology is high because of the cost of components. Alkaline electrolyzers despite their low efficiency is still the most matured and commercial technology.
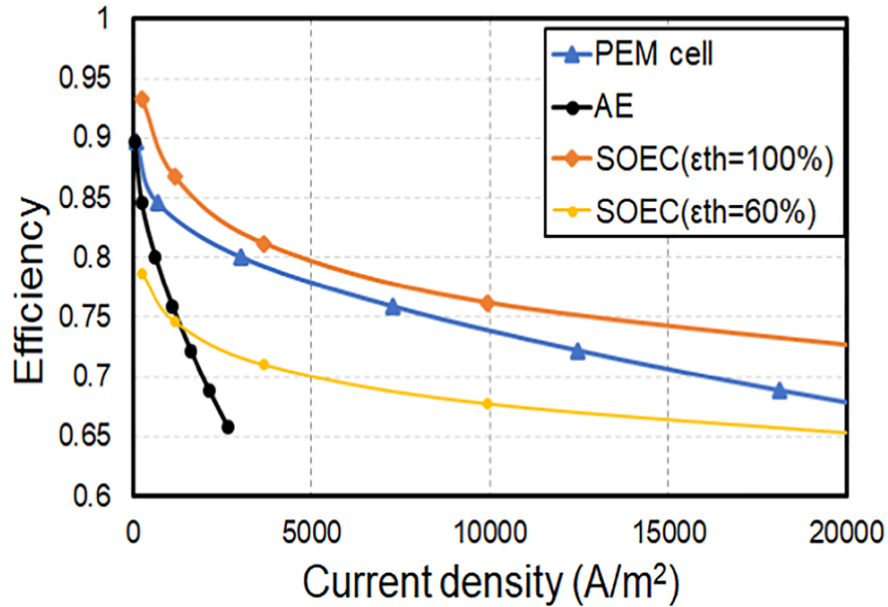
Figure 1. Efficiency comparisons of different type of electrolyzer [15].

Alkaline electrolyzers are known for their long-term stability, and cost effectiveness [17,18]. Considerable research is ongoing for improving their current density [19,20]. Figure 2 shows a commercial alkaline electrolyzer. Figure 3 shows the typical configuration of alkaline electrolyzers. The electrolyte is pumped through the electrolysis cell generating H_2 and O_2. Electrolytes are then sent to gas separators removing gases from the liquid phase. The liquid phase flows back to the electrolysis stack. For cathode, water makeup is provided before it is returned to cathode. Heat exchangers are used in the electrolyte return lines for maintaining the desired temperature.

Figure 2. Hydrogenic Commercial Alkaline Water Electrolyzer [16].
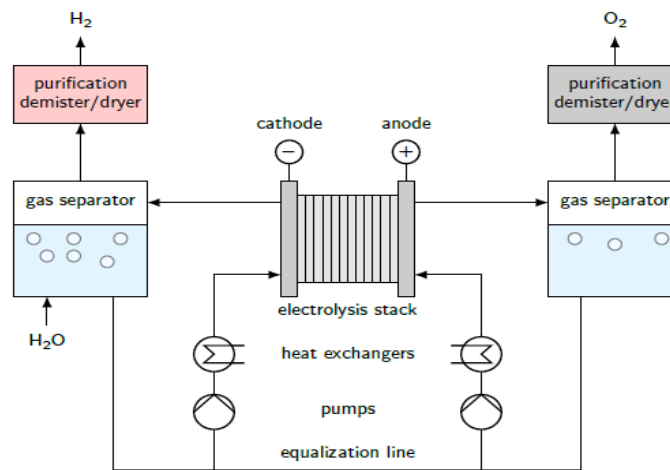
Figure 3. A schematic flow diagram of an alkaline water electrolyzer [21].

Geogios et. al. developed a mathematical model of the dynamic energy and mass balance of an industrial scale alkaline electrolyzer [22]. Several other modeling studies for alkaline electrolyzers have been reported [22,23,24]. Techno-economics analysis of electrolyzers is an important area of work for evaluating their commercial feasibility [25]. Matute, et. al. conducted an advanced techno-economic analysis of water electrolyzers to determine the optimal dispatch of the large scale electrolyzer plants to access the business feasibility of production and utilization of hydrogen for different purposes [26]. International Renewable Energy Agency (IRENA) presented a cost analysis for green hydrogen production [26]. Figure 4 shows a summary of their results.

Several other studies focusing on techno-analysis with or without optimization have been presented in the literature [26,27,28,29,30]. There is hardly any work on optimal hydrogen production and utilization especially with hydrogen being the only fuel in the turbine such as in a Peaker plant.
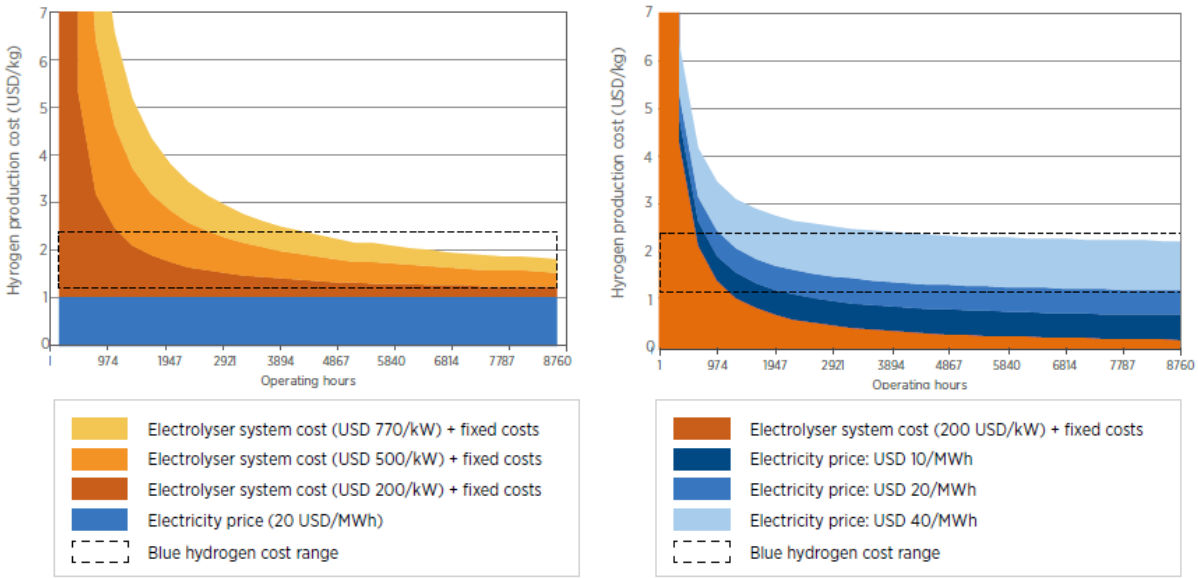
Figure 4. Hydrogen production cost as a function of investment, electricity price and operating hours [26].

1.1.3 Hydrogen Storage

Table 3 shows various options for H_2 storage. Optimal selection of hydrogen storage systems is essential for a robust hydrogen economy [29,30]. Hydrogen can be stored physically as either a gas or a liquid. Storage of hydrogen as a gas typically requires high-pressure (350–700 bar) for economic reasons. Storage of hydrogen as a liquid requires cryogenic temperatures because the boiling point of hydrogen at atmospheric condition is −252.8°C. Hydrogen can also be stored on the surfaces of solids (by adsorption) or within solids (by absorption) [29]. Compressed gas storage is the most mature technology for hydrogen storage. There are four types of high-pressure vessels used for storing hydrogen gas as listed in Table 4.

Table 3. Some known method of hydrogen storage [7]

Methods of Storing Hydrogen	
Physical-based	Compressed Gas
	Cold/Cyro Compressed
	Liquid Hydrogen
Material-based	Adsorbent
	Liquid Organic
	Interstitial hydride
	Complex hydride
	Chemical hydrogen

Table 4. Type of Vessels for Storing Hydrogen as a Compressed gas

Type I	Pressure vessel made of metal
Type II	Pressure vessel made of thick metallic liner hoop wrapped with a fiber-resin composite
Type III	Pressure vessel made of a metallic liner fully wrapped with a fiber-resin composite
Type IV	Pressure vessel made of polymeric liner fully wrapped with a fiber-resin composite. The port is metallic and integrated into the structure

The decision on which vessel to use for hydrogen storage depends on the final application of hydrogen. Even though Type III and Type IV have the potential to store hydrogen at a very high pressure and small volumes, they are often used in mobile systems because of their seemingly light weight. To build a Type I vessel (which is the cheapest and most common) of high pressure of about 300 bar, the weight of the vessel is generally high, which is acceptable for stationary application. The vessel type selection is a compromise between technical performance and cost-competitiveness [6]. There are multiple papers in the literature on the economic model of hydrogen storage [8,29,30,31,32,33]. Most of the works presented in the literature are based on the vendor quotes and therefore not suitable for optimizing the vessel design conditions. In this research,

vessels are sized with due consideration of the stress and capacity and their costs are calculated by considering pressure and material factor as well as commercial data thus making it suitable for NPV optimization.

1.2 NPV Optimization for Optimal Design and Operation of Flexible NGCC Plants with CO_2 Capture Plant and Hydrogen Generation and Utilization

Flexible operation of capture plants integrated with power plants has been investigated by various researchers. Cheng et al. [34] modelled flexible operation of an NGCC plant coupled with a carbon capture plant. An intensive energy analysis with and without carbon capture system has been conducted for a power plant [35]. Mores et al. [36] optimized an integrated NGCC plant with a CO_2 capture plant by evaluating different configurations. Monoethanolamine (MEA) was used as the solvent. Multi-objective optimization was done for a CO_2 capture plant integrated with a power plant investigating cost of avoided CO_2 emission and energy [37]. Operational optimization of amine-based post carbon capture (PCC) process at part load condition has been reported by Litzelman et.al [38]. Net present value (NPV) optimization has been undertaken by several researchers by taking into account both capital and operating costs. Zantye et al. [39] applied a two-stage optimization approach for optimal design and operation of a coal-fired unit integrated with onshore wind and solar photovoltaics (PV) fields. Yuan et al. [40] conducted modeling and optimization of a membrane-based carbon capture plant interagted with an NGCC plant. Economic optimization of a CO_2 capture plant based on the day ahead locational marginal price (LMP) of electricity has been reported [41]. Amount of carbondioxide emission at different carbon prices is presented. Oates et al. [41] considered year long LMP to investigate the profitability of a power plants integrated with PCC. They performed a study to determine whether flue gas bypass and solvent storage can increase the profitability of a power plant integrated with PCC. Their study shows that benefits of flexible carbon capture and storage (CCS) reduce as price of CO_2 emission increases. Bandyopadhyay et.al. [42] investigated optimal configuration and operation, profits, cost of CO_2 capture, and levelized cost of electricity for a hybrid system, with and without considering the constraints on the variability of the net power output. However, there is hardly any study in the existing literature on NPV optimization of a NGCC plant integrated with a post combustion carbon capture technology considering flexible capture with variable yearly LMP and carbon tax.

Hydrogen is being widely investigated as a clean fuel. A gas switching reforming technology has been proposed in [43]. H_2 is generated both by methane steam reforming as well as by electrolysing the steam generated from the power plant with integrated PCC plant. Cloete et al. [44] compared the feasibilty and economic benefits of different hyrogen production routes. Zhang & Zhang [45] evaluated an integated power plant, PCC and hydrogen generation unit where H_2 is generated by alkaline electrolysers. Figure 5 shows a NGCC power plant integrated with a PCC plant, and units for hydrogen production and storage. Co-firing of H_2 and natural gas in the gas turbine (GT) is assumed to be acceptable till 20 wt% of H_2. To the best of our knowledge, there is no work on NPV optimization in the existing literature for such a configuration. In this research, NPV optimization of this integrated system is undertaken for optimal design and operation of the integrated system shown in Figure 5.
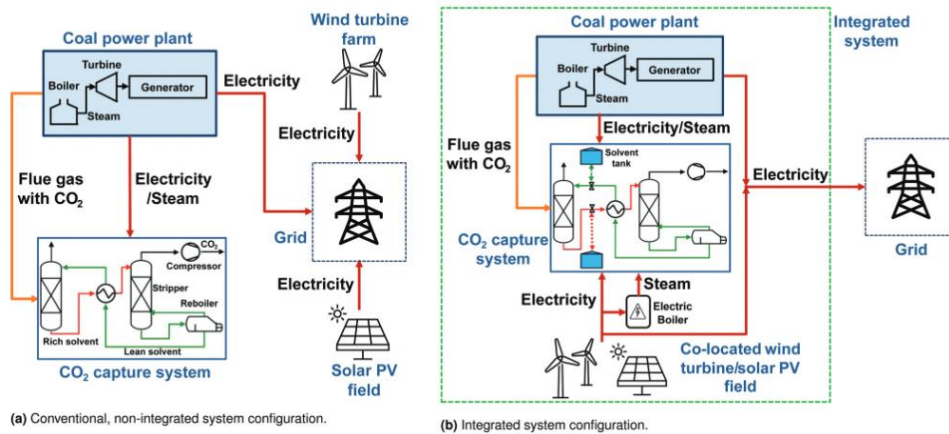
Figure 5. Schematic of a NGCC plant integrated with carbon capture, hydrogen storage and injection [39].

A review of publicly available data for thermal peaking plant was done in [46]. They presented the obtainable capital and operating expenditure cost estimates at various nominal capacities for both gas and liquid fired Peaker plants. Jeffrey [47] provided update on the economic implication and operational feasibility of gas turbine operating on high hydrogen content fuel. He presented different plants that are currently operating on almost 100% hydrogen fuel while discussing the benefits and challenges of using such high content of hydrogen as fuel in the gas turbine. The efficiency of a simple cycle plant was studied in comparison of the power output of a high efficiency Peaker plant [48]. The performance of the plant based on the unique feature of the

plant were recorded and it gave a good insight into some operational characteristics of simple cycle gas turbine. No work has been done on the optimization of a Peaker plant that utilizes 100% hydrogen with the inclusion of hydrogen generation and storage and this is one of the gaps we wish to fill in this work.

1.3 Clustering for Obtaining Representative Days

For NPV optimization of power generation systems, electricity price needs to be considered. Electricity price can change at the timescale of minutes to hours, and can have high frequency and volatility, varying mean and variance, multiple seasonality and calendar effects [49]. Therefore, for optimal design and operation of power production systems, large time span that can include months to years should be considered resulting in a computationally expensive problem for NPV optimization. Hence, representative time periods that can characterize a group of hours or days can be very useful. Various types of clustering algorithms have been developed to obtain these representative hours/days [50,51]. Warren [52] provided a survey of works that has been done in time series clustering across many applications. Dongkuan et al. [53] carried out a comprehensive survey on clustering algorithm and their selection criterions. Dissimilarity(distance) and similarity are the two most important basis for building an algorithm for clustering. It was reported in [54] that similarity is preferred when dealing with qualitative data while distance is most desired when dealing with quantitative data. Two primary approaches for clustering are hierarchical clustering and partitioning clustering. These approaches and their subclassifications are shown in Figure 6.
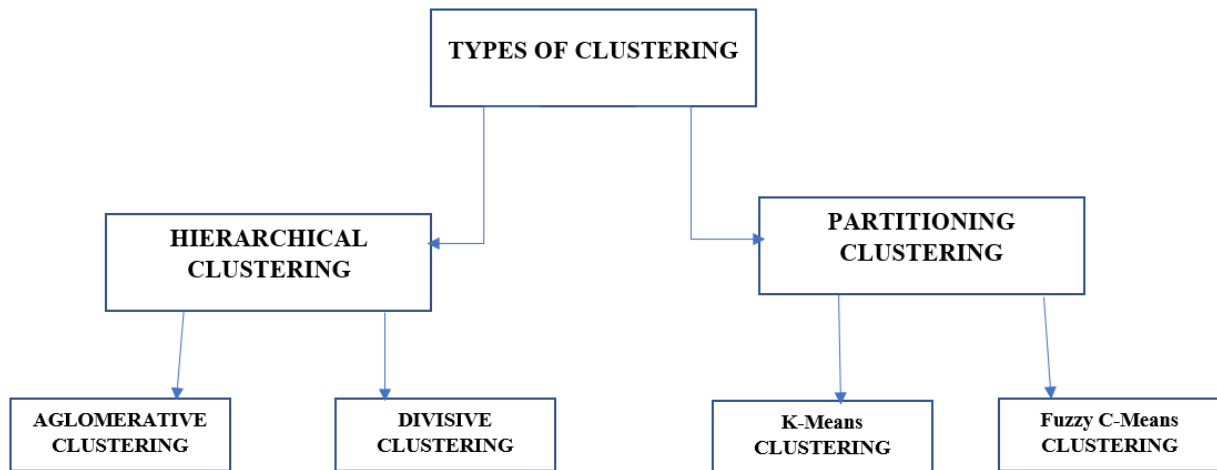
Figure 6. Categorization of clustering methods.

Partitioning around medoids (PAM), which is a type of k-means approach [55], has been one of the most popular and latest clustering approaches for time series electricity prices. There are however two shortcomings with the PAM method. Firstly, it can result in different clusters for different runs on the same dataset. Also, it is difficult to obtain the best k value that affects the quality and number of clusters. Hierarchical clustering results in a cluster that is easier to understand due to its top-bottom or bottom-top approach. The hierarchical clustering analysis also explores (dis)similarity in data points. Some of the commonly used metrics to explore the (dis)similarity through distance between datapoints have been discussed [51,56]. A distance function based on derivative for measuring similarity was proposed by Górecki & Łuczak [57]. They explored the derivative distance of both the Euclidean distance and the dynamic data warping. Table 5 represents some popular distance function that are currently in use [51]. For a clustering approach to be used for decision making for optimal operating conditions, it is desired that two days are clustered when for each matching hour in those days, absolute differences and relative differences in LMP are within some tolerance. Since power plant needs to ramp up or down based on the LMP, for clustering another important criterion would be similarity in rate of change in relative price. These criteria for clustering have not been used currently in the existing literature.

Table 5. Distance Measure for Clustering Algorithms [53]

Name	Formula	Explanation
Minkowski distance	$(\sum_{l=1}^{d} |x_{il} - x_{jl}|^n)^{\frac{1}{n}}$	A set of definitions for distance: 1. City-block distance when n=1 2. Euclidean distance when n=2 3. Chebyshev distance when n tends to ∞
Standard Euclidean distance	$\left(\sum_{l=1}^{d} \left|\frac{x_{il} - x_{jl}}{S_l}\right|^2\right)^{1/2}$	1. S is standard deviation 2. A weighted Euclidean distance based on deviation
Cosine distance	$1 - \cos \propto = \dfrac{x_i^T x_j}{||x_i|| \, ||x_j||}$	1. Stay the same in the face of the rotation change of data 2. The most used distance in document area
Pearson Correlation distance	$1 - \dfrac{Cov(x_i, \, x_j)}{\sqrt{D(x_i)}\sqrt{D(x_j)}}$	1. Cov is the covariance while D is the variance 2. Measure the distance based on linear correlation
Mahalanobis distance	$\sqrt{(x_i - x_j)^T S^{-1}(x_i - x_j)}$	1. S is the covariance matrix inside the cluster 2. It has high computation complexity

Chapter 2

LMP Clustering Algorithm

2.1 Development of a clustering algorithm for the LMP of different regions (Objective#1)

The objective of this part of research are to develop a clustering algorithm to reduce the number of days to be considered for NPV optimization of the integrated plant. Each of the region considered for the NPV optimization has hourly data for the entire year. In this work, the following two-level clustering approach is proposed. In this approach, number of clusters are not pre-specified like typical c-means or k-means clustering approaches but are rather computed depending on the suer specified tolerance. Level 1 criteria are based on some form of distance measure between the prices at a given hour in a day with the same hour in another day. For distance measure, we consider absolute differences and relative differences in LMP between two days. Considering the LMP is available for each hour in a day, first %relative difference between each hour in a day with the same hour in another day is considered as shown in Eq. (1). The mean of the absolute %relative differences is computed as shown in Eq. (2) and considered as a criterion in Level 1. We also calculate the absolute differences between each hour in a day with the same hour in another day as shown in Eq. (3) and compute the max for all hours and use that as another criterion for Level 1.

$$C_{i,j,k} = \left(\frac{P_{i,j} - P_{k,j}}{Max(P_{i,j}, P_{k,j})} \right) \quad i \# k; i, k = [1,2,..365], j = [1,2,..24] \tag{1}$$

$$Q_{i,k} = \frac{\sum_{j=1}^{24} abs(C_{i,j,k})}{24} \tag{2}$$

$$D_{i,j,k} = abs(P_{i,j} - P_{k,j}) \quad i \# k; i, k = [1,2,..365], j = [1,2,..24] \tag{3}$$

$$S_{i,k} = \max(D_{i,j,k}) \tag{4}$$

$$P_{i,j}, P_{k,j} \geq 0 \tag{5}$$

If $Q_{i,k} \leq \epsilon_1$ and $S_{i,k} \leq \epsilon_2$, i and k are similar.

Level 2 similarity is computed to determine similarity of LMP between two consecutive hours. As LMP is a key criterion for the ramp changes in load of a power plant, this criterion ensures that the expected dynamics in load, operation of the capture plant and H_2 generation and storage systems are similar. It should be noted that in this work on NPV optimization, a dynamic optimization problem is solved considering the dynamics of the integrated system. Therefore, Level 2 similarity is used to ensure that it is not only the similarity of LMP between two specific hours but between two consecutive hours are considered for clustering. Relative differences in LMP for all consecutive hours are computed for any given day and another candidate day and then their differences are computed as shown in Eq. (5).

$$R_{i,j,k} = abs\left(\left(\frac{P_{i,j+1} - P_{i,j}}{max(P_{i,j+1}, P_{i,j})}\right) - \left(\frac{P_{k,j+1} - P_{k,j}}{max\ (P_{k,j+1}, P_{k,j})}\right)\right) \qquad (6)$$

For all j, if max $(R_{i,j,k}) < \epsilon_3$ and $avg(R_{i,j,k}) < \epsilon_4$, i and k are similar. It should be noted that as the tolerances are all inclusive for determining if two days will be clustered, all four tolerances can be considered together without separating them in two levels. We observed that if only Level 1 tolerances are considered first then large number of days are eliminated from further consideration thus saving computational cost for computing the measures required for Level 2 consideration. There are four user specified tolerances-$\epsilon_1, \epsilon_2, \epsilon_3, \epsilon_4$. The tolerance ϵ_2 has a \$/MWh value, while the tolerances ϵ_1, ϵ_3, and ϵ_4 are dimensionless. Once all clusters are determined, then for each cluster, mean LMP for each hour is computed by considering LMP at that hour for all member days in that cluster. The mean for each hour then represents each cluster and is used for NPV optimization.

2.2 LMP Data Scenarios

Two types of data scenarios were considered in this work. Data from NREL provides electricity price for five regions under two different CO_2 tax condition (\$100/ton CO_2 and \$150/ton CO_2). This gives a total of 10 different prices. Data from Princeton considers \$60/ton CO_2 tax for four different cases. The four conditions provided in the Princeton data are base case, high wind case, high solar and winter. The clustering algorithm discussed above is applied to LMP data sets for these 14 scenarios.

2.3 Results & Discussion for the LMP Clustering Algorithm

Sensitivities to all tolerances are evaluated and results are presented below for a selected six scenarios in NREL case and all the four scenarios in the Princeton case.

Impact of Change in ϵ_1

ϵ_1 is varied from 5% to 100% (0.05 to 1). Other three tolerances are fixed: $\epsilon_2 = \$20/MWh$, $\epsilon_3 = 40\%$, $\epsilon_4 = 20\%$. The result was presented in Figures 7a and 7b for NREL and Princeton cases, respectively. Below some value of ϵ_1, it becomes the limiting criterion and therefore number of cluster days increase rapidly with reduction in ϵ_1. When ϵ_1 is relaxed, the number of cluster days do not change as much.

(a)   (b)
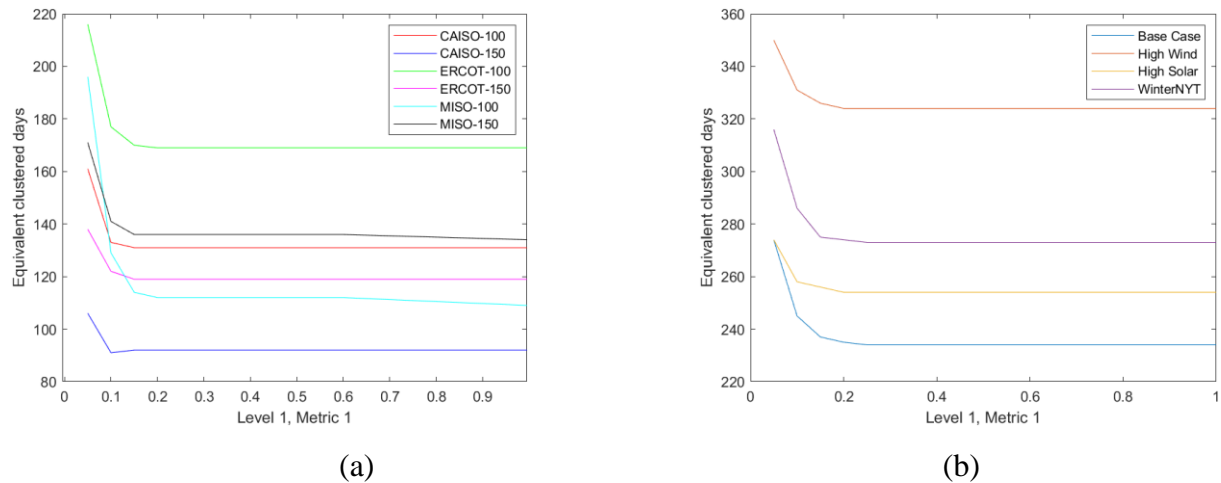
Figure 7. Plot of equivalent days versus tolerance 1 for (a) NREL cases, (b) Princeton cases.

Impact of Change in ϵ_2

ϵ_2 was varied between \$5-\$100/MWh while keeping other three tolerances fixed at: $\epsilon_1 = 20\%$, $\epsilon_3 = 40\%$, $\epsilon_4 = 20\%$. Figures 8a and 8b show results for NREL and Princeton cases, respectively. While the results are similar to before for most of the cases, for Princeton Base Case, the number of clustered days kept reducing till when ϵ_2 reached a value of \$100/MWh.

| (a) | (b) |
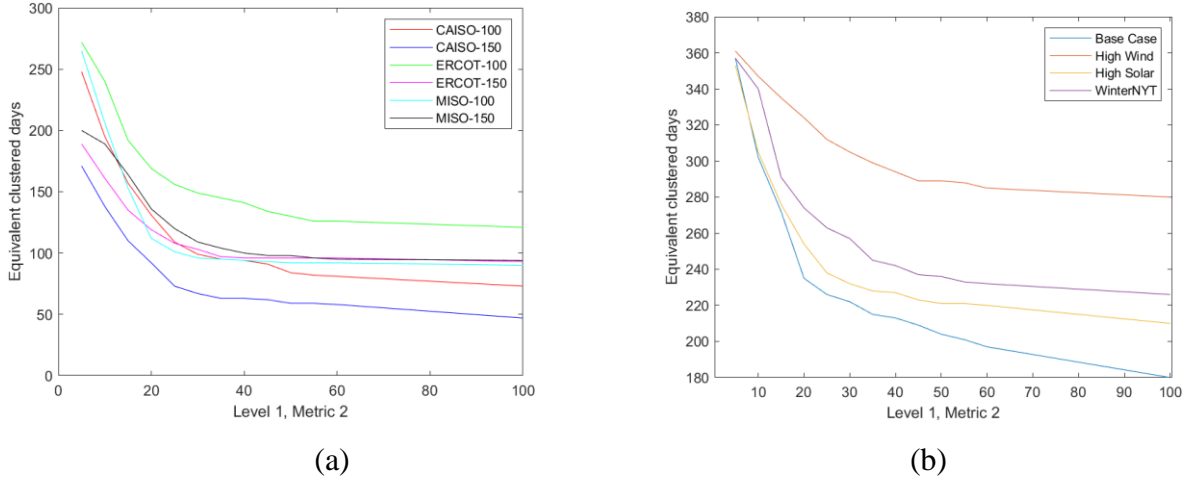
Figure 8: Plot of equivalent days versus tolerance 2 for (a) NREL cases, (b) Princeton cases.

Impact of Change in ϵ_3

ϵ_3 is varied from 5% to 100% (0.05 to 1) keeping other tolerances fixed: $\epsilon_1 = 20\%$, $\epsilon_2 = \$20$, $\epsilon_4 = 20\%$. The result was presented in Figures 9a and 9b for the NREL and Princeton cases, respectively. Interestingly it is observed that for all Princeton cases, this criterion plays a limiting role even till a value of 100%.

| (a) | (b) |
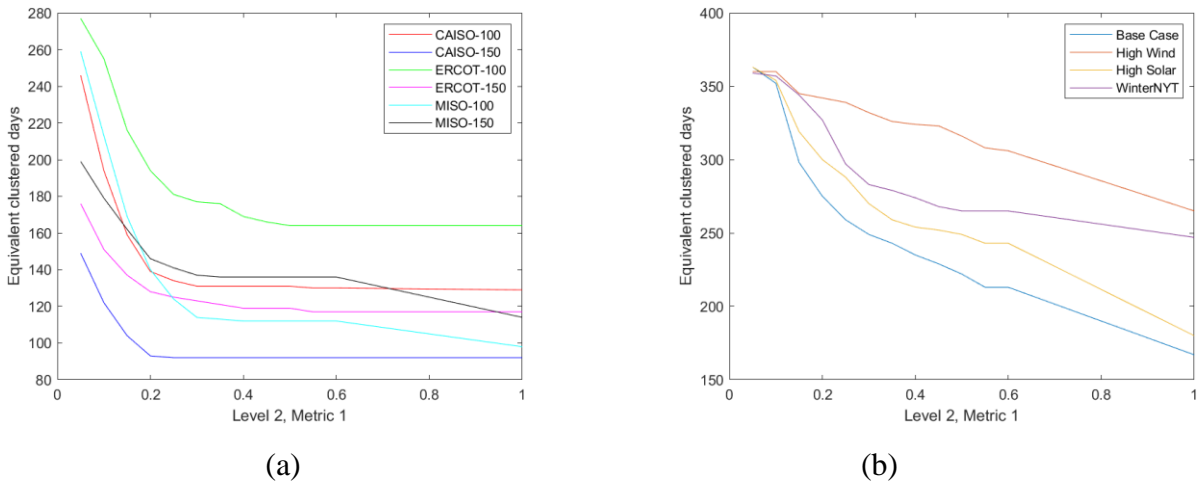
Figure 9. Plot of equivalent days versus tolerance 3 for (a) NREL cases, (b) Princeton cases.

Impact of Change in ϵ_4

ϵ_4 was varied from 5-100% (0.05 to 1). Three other tolerances were kept fixed at: $\epsilon_1 = 20\%$, $\epsilon_2 = \$20/MWh$, $\epsilon_3 = 40\%$. Results are presented in Figures 10a and 10b for the NREL and

Princeton cases, respectively. This tolerance is found to have the least impact out of all tolerances on number of cluster days.
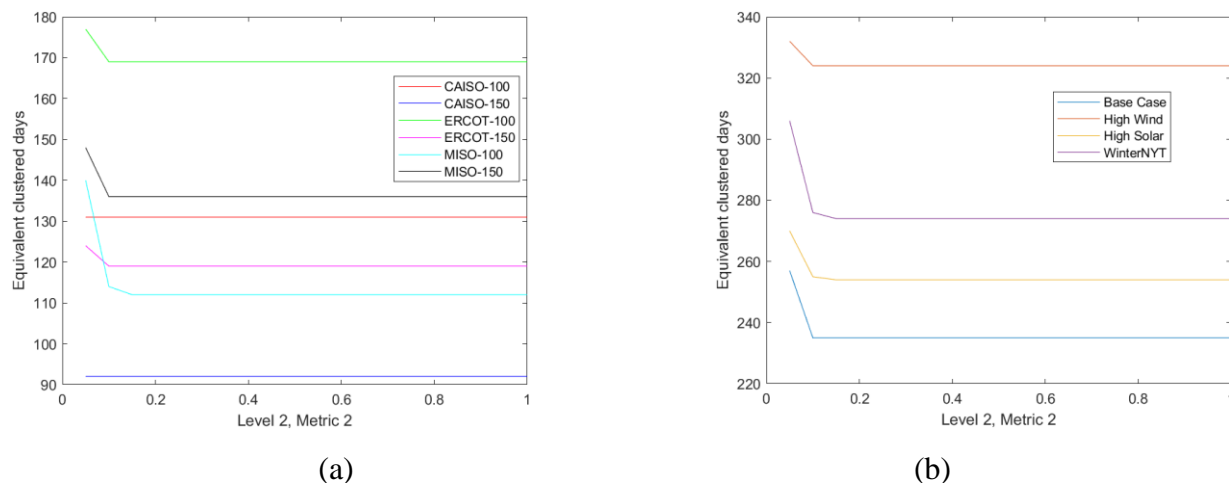
Figure 10. Plot of equivalent days versus tolerance 4 for (a) NREL cases, (b) Princeton cases.

Using the results presented above and by considering the resulting number of cluster days, final values of tolerances for each region are set as shown in Table 6. It is observed that there is only modest reduction in number of (equivalent) days for Princeton cases.

Table 6. Final Tolerance Value Used for Each Region

	$\epsilon_1(\%)$	ϵ_2 ($/MWh)	$\epsilon_3(\%)$	$\epsilon_4(\%)$	Equivalent Days
CAISO_100	15	20	30	5	131
CAISO_150	15	20	25	5	92
ERCOT_100	20	20	40	10	169
ERCOT_150	15	20	40	10	119
MISO_100	20	20	40	15	112
MISO_150	15	20	35	10	136
NYSIO_100	20	20	40	10	140
NYSIO_150	15	20	30	10	126
PJM_100	20	20	40	10	184
PJM_150	20	20	40	10	196
BaseCase_60	20	20	40	10	235
HighWind_60	20	20	40	10	324
HighSolar_60	20	20	40	15	254
WinterNYT_60	20	20	40	15	274

Chapter 3

Model Development, Validation and Optimization for CO_2 Capture and H_2 Generation and Utilization Process Integrated with NGCC Plant

3.1 Development of Reduced Order Models (Objective#2)

As the NPV optimization is a dynamic optimization problem and it needs to be solved for large number of time periods, use of detailed nonlinear models is computationally expensive. Therefore, reduced order models are developed and used for NPV optimization.

3.1.1 CO_2 Compression System

For developing the reduced order model of the CO_2 compression system, the detailed CO_2 compression system model developed by Modekurti et al. [58] is considered. The rigorous model was developed in Aspen Custom Modeler (ACM) using the Lee-Kesler-Plocker thermodynamic package for compressors, coolers, and flash drums [59]. Figure 11 represents the flowsheet for the mode that also includes the triethylene glycol (TEG) dehydration system.
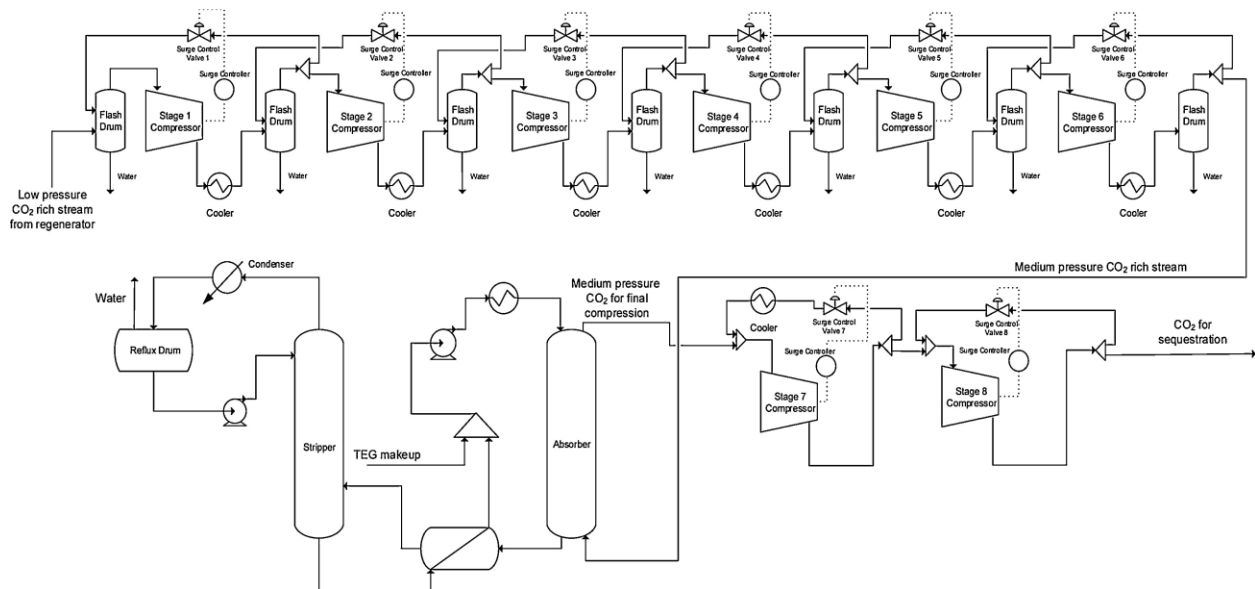
Figure 11. Flowsheet of the CO_2 compression train [58].

While developing the reduce model, it is assumed that the H_2O mole fraction in the final outlet stream does not vary due to the presence of a TEG dehydration system. The TEG absorber

system is shown in detail in Figure 12. The CO_2 compressors system has a total of 8 stages of compression, The first 6 compressors have interstage coolers and flash separator for removing water. For removing moisture in the final CO_2 to about 130 ppm, the TEG absorber system is used.
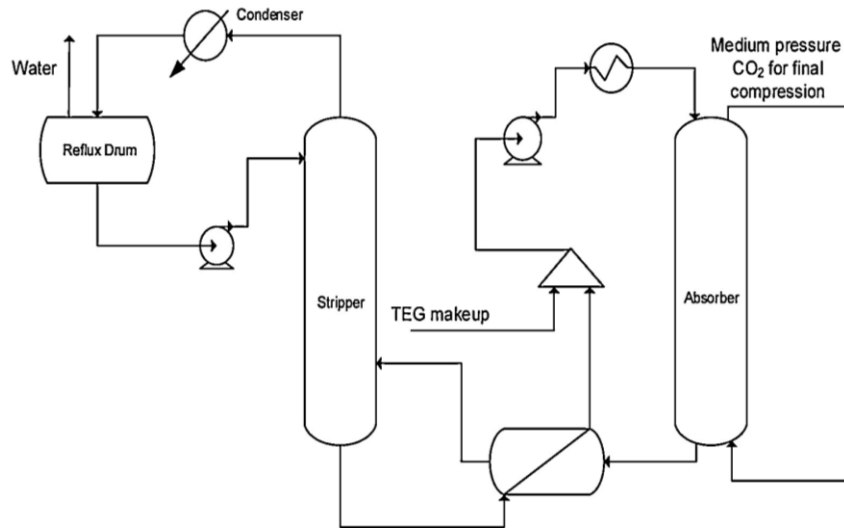
Figure 12. TEG dehydration system flowsheet [58].

3.1.2 Data Generation and Scaling

For the reduced model, the input variable is the CO_2 flowrate at the inlet while the output variables are the power consumption in 8 compressors, the cooling duty of the 6 interstage coolers, and the final flowrate of CO_2 to the storage. To generate the input-output data, 20 Latin hypercube sampling of the input variables were generated in the range of 0-1. These samples were converted to the appropriate units for simulating the Aspen model as shown in Eq. (7).

$$U_i = lhs_{sample,i}(U_i max - U_i min) + U_i \min \qquad (7)$$

Where U_i is the input passed into the ACM in order to generate the 15 output variables. $U_i max$ and $U_i min$ are the upper and the lower bound of the desired flowrate range respectively while $lhs_{sample,i}$ is the corresponding Latin sample value for flowrate U_i. The output variable of interest and their unit are shown in appendix 1. Input and output variables are scaled as shown in Eqs. (8)-(10) and the variables are listed in Table 7.

$$u_i = \frac{CO_2 \; flowrate \; to \; storage_i \frac{kmol}{hr}}{Maximum \; CO_2 \; flowrate \; to \; storage, \; \frac{kmol}{hr}} \tag{8}$$

$$y_k = \frac{Cooling \; Duty \; of \; Cooler_k, \frac{MJ}{hr}}{CO_2 \; flowrate \; to \; storage_k, \frac{kmol}{hr}} \tag{9}$$

$$y_k = \frac{Power \; Consumption \; in \; Compressor_k, \frac{MJ}{s}}{CO_2 \; flowrate \; to \; storage_k, \frac{kmol}{hr}} \; 3600 \tag{10}$$

Table 7. Scaled Output Variables and Units

Output (y)	Variable Name	Unit
y1	Cooling Duty in Interstage Cooler 1	MJ/kmol
y2	Cooling Duty in Interstage Cooler 2	MJ/kmol
y3	Cooling Duty in Interstage Cooler 3	MJ/kmol
y4	Cooling Duty in Interstage Cooler 4	MJ/kmol
y5	Cooling Duty in Interstage Cooler 5	MJ/kmol
y6	Cooling Duty in Interstage Cooler 6	MJ/kmol
y7	Power Consumption in Compressor Stage 1	MJ/kmol
y8	Power Consumption in Compressor Stage 2	MJ/kmol
y9	Power Consumption in Compressor Stage 3	MJ/kmol
y10	Power Consumption in Compressor Stage 4	MJ/kmol
y11	Power Consumption in Compressor Stage 5	MJ/kmol
y12	Power Consumption in Compressor Stage 6	MJ/kmol
y13	Power Consumption in Compressor Stage 7	MJ/kmol
y14	Power Consumption in Compressor Stage 8	MJ/kmol

All candidate models considered in this work are linear in parameter but can be linear or nonlinear in terms of variables. Equation 11 shows a generic linear in parameter model, where H denotes the parameter vector, X denotes regressors, Y denotes regressed. and Eq. 12 yields the ordinary least squares estimate of the parameter vector.

$$Y = XH \tag{11}$$

$$H = (X^T X)^{-1} X^T Y \tag{12}$$

3.1.3 Model Evaluation

  Various statistical measures are used to evaluate the goodness of fit. R^2, RMSE and MPE are some of the traditional measures given by Eq. (13)-(17), but these measures do not necessarily indicate overfitting. Akaike information criterion (AIC) and Bayesian information criterion (BIC), given by Eqs. (18)-(20) can indicate overfitting where an increase in the size of the model parameters represented by K is used as a penalty term [60]. For simplicity, TSE, given by Eq. (20) is used as the likelihood function in this work.

$$R_k^2 = 1 - \frac{SS_{res,k}}{SS_{tot,k}} \tag{13}$$

$$SS_{tot,k} = \sum_k (y_{k,i} - mean_k)^2 \tag{14}$$

$$SS_{res,k} = \sum_k (y_{k,i} - y_{m,i})^2 \tag{15}$$

$$RMSE_k = \sqrt{\frac{\sum_{i=1}^N (y_{k,i} - y_{m,i})^2}{N}} \tag{16}$$

$$MPE_k = \sqrt{\frac{1}{N}\sum_{k=1}^N \left[\frac{(y_k, i - y_{m,i)}}{y_{k,i}} * 100\right]^2} \tag{17}$$

$$AIC_k = Nln\left(\frac{TSE_k}{N}\right) + 2K \tag{18}$$

$$BIC_k = Nln(TSE_k) + KlnN \tag{19}$$

$$TSE = \sum_k (y_{k,i} - mean_k)^2 \tag{20}$$

3.1.4 Result of Linear Model Developed

The linear model is generally of the form presented by Eqn 21. The two parameters being estimated here are c_k and a_k. Table 8 lists R^2, RMSE, and MPE for all outputs. The variables marked in red are not considered to be acceptable as reflected by their low R^2, and/or high RMSE and/or MPE.

$$y_k = c_k + a_k u_1 \qquad\qquad (21)$$

Table 8. Evaluation of the Model

Output Models	R^2	RMSE (MJ/kmol)	MPE (%)
y1	0.88	0.05	0.98
y2	0.45	0.01	0.21
y3	0.98	0.01	0.15
y4	0.93	0.00	0.13
y5	1.00	0.00	0.12
y6	0.99	0.01	0.34
y7	0.50	0.00	0.07
y8	0.60	0.01	0.24
y9	0.86	0.01	0.30
y10	1.00	0.00	0.04
y11	1.00	0.00	0.13
y12	1.00	0.01	0.34
y13	1.00	0.00	0.01
y14	0.99	0.00	0.23

Results comparing the ACM data with the linear fit are presented in Figure 2A (1-14) in APPENDIX II. Only two figures are shown in Figure 13 where Figure 13a shows the comparison for the specific cooling duty of Cooler 2 (y_2) indicating that the linear fit is unacceptable while Figure 13b shows the comparison for specific duty of compressor Stage 5 (y_{11}) indicating an excellent fit.
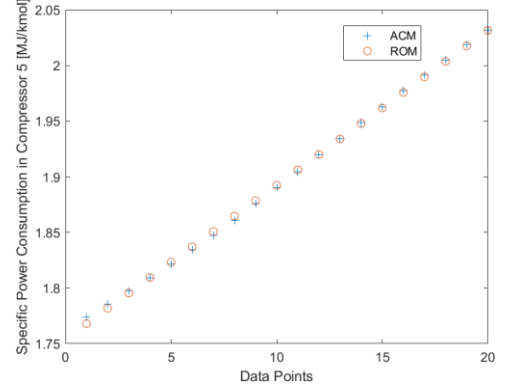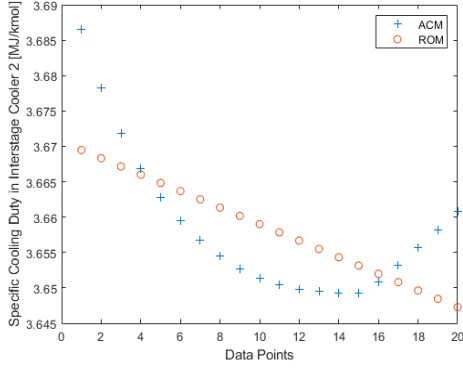
Figure 13. Plot of a good and bad linear fit for the output model, (a) Specific cooling duty in Cooler 2, (b) Specific power consumption in compressor Stage 5.

3.1.5 Result of the Nonlinear Reduced Model

For the 6 output variables where the linear model was not acceptable, nonlinear quadratic and cubic models given by Eqs. 22 and 23 respectively are evaluated. The cubic model was used only for y_7 while the quadratic model was found to be sufficient for the remaining 5 variables, i.e., y_1, y_2, y_4, y_8, y_9. Table 9 summarizes the statistical measures shown in green for these 6 variables.

$$y_k = c_k + a_k u_1 + b_k u_1^2 \tag{22}$$

$$y_k = c_k + a_k u_1 + b_k u_1^2 + d_k u_1^3 \tag{23}$$

Table 9. Model Evaluations of the Models Including the Nonlinear improvement

Output Model	R^2	RMSE (MJ/kmol)	MPE (%)
y1	0.98	0.02	0.39
y2	0.99	0.00	0.03
y3	0.98	0.01	0.15
y4	1.00	0.00	0.00
y5	1.00	0.00	0.12
y6	0.99	0.01	0.34
y7	0.95	0.00	0.02
y8	1.00	0.00	0.02

Table 9 Cont'd. Model Evaluations of the Models Including the Nonlinear improvement

Output Model	R2	RMSE (MJ/kmol)	MPE (%)
y9	0.99	0.00	0.09
y10	1.00	0.00	0.04
y11	1.00	0.00	0.13
y12	1.00	0.01	0.34
y13	1.00	0.00	0.01
y14	0.99	0.00	0.23

Figure 2B (1-6) in APPENDIX II shows the updates fits for these 6 variables. As an example of the improvement due to the nonlinear model, Figures 14a and 14b compare the fit of the linear and nonlinear models for y2 indicating the considerable improvement due to the nonlinear term. Table 10 lists the model coefficients of the final models for all output variables.
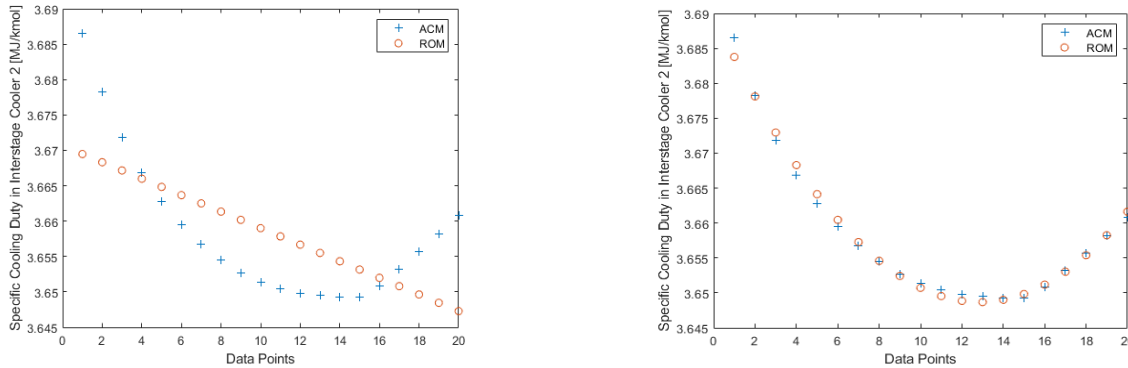
Figure 14. Comparison of the ACM data and model fit for specific cooling duty in cooler 2 (y_2) (a) Linear model, (b) Nonlinear model.

Table 10. Model Parameters for the Compressor ROM Developed

k	a_k	b_k	c_k	d_k
1	-4.239	22.962	-13.929	0
2	5.64	-4.310	2.32	0
3	2.452	0.536	0	0
4	3.283	-1.682	1.047	0
5	0.984	1.738	0	0
6	2.096	1.734	0	0
7	11.235	-27.122	30.50	-11.423
8	5.346	-4.508	2.41	0
9	0.477	4.644	-2.394	0
10	2.434	-0.227	0	0

3.1.6 Development of ROM for the TEG Dehydration

Like the reduced model of the CO_2 compressor system, input-output data are generated from the ACM model [58]. Input and output variables are listed in Tables 11 and 12, respectively, and output variables are scaled as shown in Eqns. 24 – 28.

Table 11. Input Variable for the TEG dehydration model

Input Variable	Description	unit
u_1	TEG Flowrate	mol/s
u_2	TEG Temperature	°C
u_3	CO2 Flow at Absorber Inlet	kmol/s
u_4	H2O Flow at Absorber Inlet	mol/s
u_5	Feed Temperature	°C

Table 12. Actual output variable for the TEG dehydration system

Actual Output Variables	Descriptions	Units
ya1	CO_2 Absorber outlet flow	mol/s
ya2	H_2O from Stripper	mol/s
ya3	CO_2 flowrate loss from Stripper	mol/s
ya4	H_2O mole fraction in Dry GAS	ppmw
ya5	Reboiler Duty	MJ/s

$$ys_1 = \frac{CO_2 \text{ absorber Outlet flow}, \frac{mol}{s}}{CO_2 \text{ Flow at Absorber Inlet}, \frac{mol}{s}} \qquad (24)$$

$$ys_2 = \frac{H_2O \text{ Flow From Stripper Outlet flow}, \frac{mol}{s}}{H_2O \text{ Flow from Absorber Inlet}, \frac{mol}{s}} \qquad (25)$$

$$ys_3 = \frac{CO_2 \text{ flowstripper outlet} \frac{mol}{s}}{CO_2 \text{ Flow at Absorber Inlet}, \frac{mol}{s}} * 100 \qquad (26)$$

$$ys_4 = ya_4 \qquad (27)$$

$$ys_5 = \frac{\text{Reboiler Duty}, \frac{MJ}{s}}{H_2O \text{ Flow at Absorber Inlet}, \frac{mol}{s}} \qquad (28)$$

The linear model for the TEG dehydration process is shown in Eq. (29).

$$ys_i = f + a_i u_1 + b_i u_2 + c_i u_3 + d_i u_4 + e_i u_5 \qquad (29)$$

Where i=1,2…5 for ys1 to ys5.

Table 13 lists statistical measures of all outputs. It is observed that the model for ys_2 and ys_4 can be improved further. Eqs. 30-34 show the candidate nonlinear models for ys_2 and ys_4.

Table 13. Model values for the TEG Dehydration system output model

Output model	R^2	RMSE	MPE
ys_1	0.98	0.00083	0.0824
ys_2	0.96	0.02	4.82
ys_3	0.98	0.083	4.76
ys_4	0.94	0.63 ppmw	0.51
ys_5	0.98	0.056 MJ/mol	4.29

$$y_{i1} = l_i + a_i u_1 + b_i u_2 + c_i u_3 + d_i u_4 + e_i u_5 + f_i u_1^2 \qquad (30)$$

$$y_{i2} = l_i + a_i u_1 + b_i u_2 + c_i u_3 + d_i u_4 + e_i u_5 + f_i u_1^2 + g_i u_2^2 \tag{31}$$

$$y_{i3} = l_i + a_i u_1 + b_i u_2 + c_i u_3 + d_i u_4 + e_i u_5 + f_i u_1^2 + g_i u_2^2 + i_i u_3^2 \tag{32}$$

$$y_{i4} = l_i + a_i u_1 + b_i u_2 + c_i u_3 + d_i u_4 + e_i u_5 + f_i u_1^2 + g_i u_2^2 + i_i u_3^2 + j_i u_4^2 \tag{33}$$

$$y_{i5} = l_i + a_i u_1 + b_i u_2 + c_i u_3 + d_i u_4 + e_i u_5 + f_i u_1^2 + g_i u_2^2 + i_i u_3^2 + j_i u_4^2 + k_i u_5^2 \tag{34}$$

Tables 14 and 15 list the statistical measures of all candidate models for ys2 and ys4, respectively.

Table 14. Model values for the nonlinear models of ys2

Output Model	y_{i1}	y_{i2}	y_{i3}	y_{i4}	y_{i5}
Number of Parameters	7	8	9	10	11
R^2	0.96	0.96	0.96	0.98	0.98
RMSE	0.02	0.02	0.02	0.02	0.02
MPE	4.81	4.82	4.82	3.61	3.59
AIC	-493.8	-491.84	-489.85	-530.25	-529.52
BIC	-475.49	-470.91	-466.31	-504.1	-500.76

Considering the results presented in Table 14, especially by considering AIC and BIC, y_{i4} is selected as the final model for ys2.

Table 15. Model values for the nonlinear models of ys4

Model	y_{i1}	y_{i2}	y_{i3}	y_{i4}	y_{i5}
Number of Parameters	7	8	9	10	11
R^2	0.98	0.98	0.98	0.98	0.98
RMSE, ppmw	0.4	0.4	0.39	0.39	0.35
MPE	0.33	0.32	0.31	0.31	0.28
AIC	110.3	109.6	105.82	107.74	86.56
BIC	128.63	130.6	129.36	133.89	115.33

Considering the results in Table 15, even though yi5 yields superior AIC and BIC compared to other models, R^2, RMSE, and MPE of all 5 models are found to be similar. Therefore, the simplest

model, i.e. y_{i1} is selected as the final model for ys_4. Table 16 lists the model coefficients for the final models of the 5 output variables.

Table 16. Model coefficients for the 5 output variables of the dehydration system

Parameters	ys1	ys2	ys3	ys4	ys5
A	-0.0004	-0.0069	0.044	-0.28	0.03
B	1.95E-05	-0.012	0.0019	0.37	0.002
C	0.017	-0.33	-1.74	-3.89	-0.032
D	0.0027	0.73	-0.27	0.46	-0.78
E	0.00055	0.012	-0.055	1.48	-0.01
F	0.96	2.23E-06	4.37	0.0028	2.17
G	0	0.00014	0	59.73	0
H	0	0.076	0	0	0
I	0	-0.1	0	0	0
K	0	0	0	0	0
L	0	-0.068	0	0	0

3.2 NPV Optimization for optimal design and operation of flexible NGCC plants with CO$_2$ capture and Hydrogen Generation, and Utilization (Objective#3)

Models for performing NPV optimization are described below.

3.2.1 NGCC

A nominal capacity of 641 MWe natural gas combined cycle (NGCC) power plant is developed and simulated in Aspen dynamics platform. A first principle model is developed based on the baseline case B31A conducted by the National Energy Technology Laboratory (NETL). The NGCC model is simulated and tested for different part load conditions and shows satisfactory performance that closely matches industry standards. The model is divided into three sections: GT, HRSG and ST. A more detailed explanation about this model can be found in [61,62]. The nonlinear model developed in Aspen Plus Dynamics (APD) in its generic form by equation 36 & 37. While equation 38 & 39 represents the continuous-time state space model is developed by linearizing the nonlinear model at both full load and part load. The state, input, and output variables are represented by $x(t), u(t), y$ respectively. The continuous-time state space model has the same

28

dimension has the aspen plus dynamic model. This model is quite large for optimization and there is need to build a reduced order model that preserves the high-fidelity on the nonlinear system.

Table 17. NGCC Model Equations

$$\dot{x} = f\big(x(t), u(t)\big) \tag{36}$$

$$y = g\big(x(t), u(t)\big) \quad ; x(t) \in R \,, u \in U \tag{37}$$

$$\dot{x} = Ax(t) + Bu(t) \tag{38}$$

$$y = Cx(t) + Du(t) \tag{39}$$

$$\dot{x_{ROM}} = A_{ROM}x(t) + B_{ROM}u(t) \tag{40}$$

$$y = C_{ROM}x(t) + D_{ROM}u(t) \tag{41}$$

$$CAPEX^{NGCC} = 571107416 \left(\frac{W}{727}\right)^n \tag{42}$$

$$OPEX^{NGCC-var} = 9292071 \left(\frac{W}{727}\right)^n \tag{43}$$

The reduced order model for the APD [59] is presented in equation 40 and 41. This reduced order model eliminates the weakly coupled states according to the tolerance limit and acceptable range of error. The high-fidelity model used for the optimization is reconfigured incorporate hydrogen stream as one of the inlets along the natural gas that is already being used. The full order model and reduced order model were also rebuilt to reflect the incorporation of the hydrogen gas as an input. The capital and operating expenditure of the NGCC are calculated using equation 43 and 44. W represents the capacity of the NGCC plant and n is the exponential scaling factor, fixed at 0.68 for this optimization.

3.2.2 PCC (Post Combustion Carbon Capture Plant)

A monoethanolamine (MEA)-based capture unit will be considered. Values for specific heating and cooling duties are obtained from Jiang et al. [11] and Zheng et al. [12]. The model equations representing the capture rate of CO_2 and the power requirement of the PCC is represented in the list of equations below.

Table 18. PCC Model Equations

$$\dot{m}_{CO_2,captured} = \alpha_{cap}\dot{m}_{CO_2} \tag{44}$$

$$\dot{m}_{CO_2,released} = \dot{m}_{CO_2} - \dot{m}_{CO_2,captured} \tag{45}$$

$$P_{pcc,reboiler} = \dot{m}_{CO_2,captured} \times Q_{pcc,reboiler} \times \eta_{reboiler} \tag{46}$$

$$P_{pcc,pump} = Q_{pcc,pump}\,\dot{m}_{CO_2,captured} \tag{47}$$

$$P_{pcc,cooler} = \eta_{cooler} \times \dot{Q}_{pcc,cooler} \times m_{CO_2,captured} \tag{48}$$

where m is mass flow rate, α_{cap} is CO_2 capture fraction, P is power consumption, Q is cooling or heating duty, and η represents the power equivalent.

3.2.3 Electrolyzer

A polymer electrolyte membrane (PEM) electrolyzer is modelled which is used to produce H_2 from water using electricity. A lumped cost model is used here which significantly cuts down on the number of variables and constraints needed to accurately model the unit. All variables and parameters being used in this model are shown in APPENDIX III. The lumped cost model allows there to be only one input and output variable, utilization and H_2 production rate, respectively, as well as a single design variable for the total capacity of the electrolyzer unit. The lower and upper bound for the unit was chosen to be 3 and 200 MW. The operating efficiency used in this model is 43 kWh/kg H_2. Only a single operating constraint is in place in this model, which is used to determine the production rate of hydrogen. This constraint is as follows:

$$H_{2,prod,t} = Elec_{cap}Elec_{util,t}\eta^{elec} \tag{49}$$

The capital cost being used, shown in Eq. (49), is approximately \$700/kW [36], which is a conservative value compared to milestone goals for electrolyzer costs, but includes total installation costs for the electrolyzer stack. The fixed operating cost is estimated at 1% of the capital cost, charged yearly.

$$CAPEX^{elec} = 704,000\,Elec_{cap} + 2,730,000 \tag{50}$$

3.2.4 Hydrogen Storage

Two stage compressors with interstage coolers and a storage vessel is considered for this system. Design and performance equations are given by Eq. 51-59. Equation 51 & 52 are used to calculate power and outlet temperature of the compressors. The cooling duty is calculated by Eq. 54. Finally, equation 55 and 56 are used for the dynamics of the hydrogen storage vessel. Equation 56 also relates the storage density and pressure using the modified ideal gas equation. To keep the whole plant an independent system on a year-to-year basis, the initial hydrogen storage density was used as a decision variable which would determine the optimal starting inventory of hydrogen at the beginning of the year. An additional constraint was then added which would ensure that the storage density at the end of the year would be consistent with the start of the year (Eq. 57). Equation 58 ensures that both injection and production of hydrogen do not take place at the same time instant.

Table 19. Hydrogen Storage System

$$P_{comp,i,t} = \left(100 z_i * \frac{k}{k-1}\right) \frac{H_{2,prod,t} R T_{i,in}}{MW_{H_2} \eta_{comp,H_2}} \left(\beta_t^{\frac{k-1}{k}} - 1\right) \tag{51}$$

$$\beta_t = \sqrt{\frac{P_{H_2,t}}{30}} \tag{52}$$

$$T_{i,out,t} = T_{i,in} \left(\frac{\beta_t^{\frac{k-1}{k}} - 1}{\eta_{comp,H_2}} + 1\right) \tag{53}$$

$$Q_{cw,i,t} = H_{2,prod,t} C_{p,H_2} \left(T_{i,out,t} - T_{i+1,in}\right) \tag{54}$$

$$\frac{d\rho_{H_2,t}}{dt} = \frac{H_{2,prod,t} - H_{2,inj,t}}{V_{H_2}} \tag{55}$$

$$\rho_{H_2,int} = \rho_{H_2,final} \tag{57}$$

$$H_{2,prod,t} \cdot H_{2,inj,t} \leq 100 \tag{58}$$

$$CAPEX^{storage} = \left(\frac{V_{H_2}}{143}\right)^{0.7} * 355{,}000 + 1{,}000{,}000 \tag{59}$$

Equation 59 denoted the CAPEX for the storage vessel where V_{H_2} is the storage volumetric capacity. The OPEX for the storage is assumed to be 1% of the CAPEX, charged annually.

All parameters and variables that are incorporated into this unit are shown in Table 3A in Appendix 3. There are no direct decision variables within this unit as the variable, $H_{2,prod,t}$, is the same value as the output variable of the electrolyzer unit.

3.3 NPV Formulation

To optimize the economics of the integrated system, maximizing the NPV was the objective function (Eq. 69). An interest rate and plant life of 7.5% and 30 years, respectively was chosen for the present worth factor shown in Eq. 60. Equation 62 shows the components of the revenue, which include net power sales to the grid (Equation 62), feed cost of natural gas, carbon tax of CO_2 emissions, revenue from selling hydrogen, and variable and fixed OPEX costs from all included units as well as plant startup costs. The term $P_{grid,t}$ is calculated by considering the difference between the gross power being generated in the NGCC plant and the power consumed in all unit operations within the system. All utility duty is converted to electrical equivalents.

Table 20. Objective function formulation for the integrated plant

$$\max NPV = P_{A,f}\,(1 - tax) \sum_{t=1}^{8760} REVENUE_t - CAPEX\left(1 - \frac{tax}{n}P_{A,f}\right) \tag{60}$$

$$P_{A,f} = \frac{(1 + i)^n - 1}{i(1 + i)^n} \cdot \frac{1}{(1 + i)^n} \tag{61}$$

$$\begin{aligned} REVENUE_t = LMP_t \cdot P_{grid,t} - C_{NG} \cdot NG_t - C_{CO_2} \cdot CO_{2,released} \\ -OPEX_{variable} - OPEX_{fixed} \end{aligned} \tag{62}$$

$$P_{grid,t} = P_{gross,t} - P_{cons,t} \tag{63}$$

$$P_{grid,t} \geq 0 \tag{64}$$

The constraints equations for the optimization have been described for each unit of the plant and it is also shown in APPENDIX III, Table 3B. Also, the optimization scheme was done for both continuous and clustered LMP profile of a selected market.

3.4 Optimization Results and Discussions

The transient profiles of the key profiles of the models are presented to better understand how the LMP is affecting the components of the integrated plant. Figure 15 shows how the NGCC power produced and the power consumption in the system change with LMP.
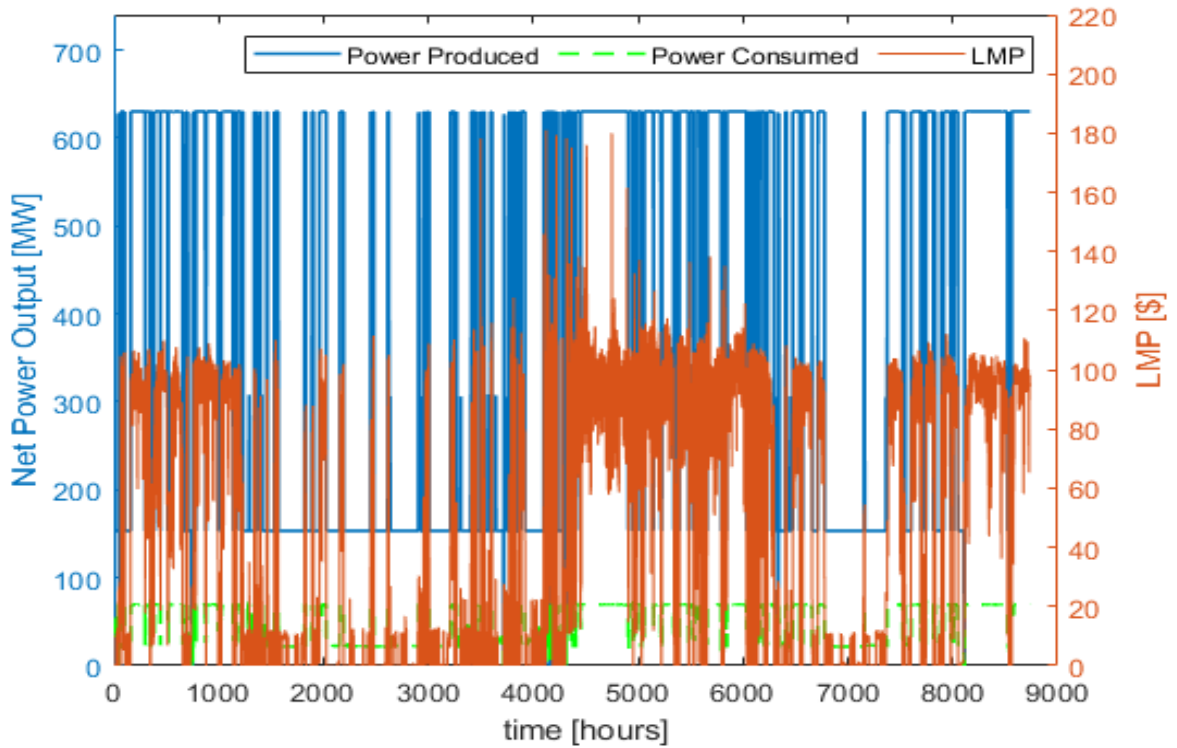
Figure 15. Power production and consumption plot for a 1-year period.

A zoomed view of the first 10 days for the power profile is shown in Figure 16. Here at a region of low LMP, the power production of the NGCC is at the lower end. This power produced is mainly used to service the power consuming sections such as electrolyzer, compressors and PCC of the integrated plant while the rest is sold off to the grid. Also, at the period of high LMP, it is more profitable to produce NGCC power at upper limit. The power consumption also increases at this level due to more power demand in components of the integrated power plant such as PCC and the CO_2 compression train.
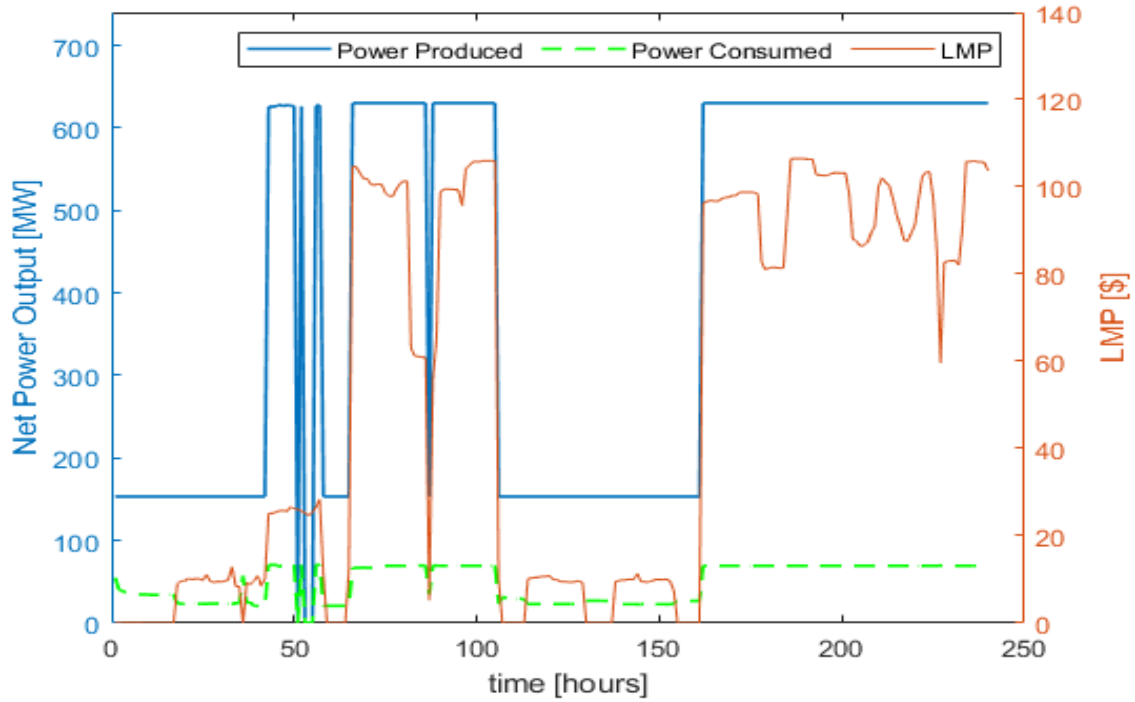
Figure 16. Power production and consumption plot for a 10 day period.

In Figure 17, the electrolyzer produces hydrogen at a period of low LMP and the hydrogen is injected into the gas turbine at a period of high LMP. The period where the LMP stays consistently high, hydrogen is neither produced nor injected because there is not enough hydrogen in the storage for injection and it is much more profitable to sell power produced to grid rather than producing hydrogen with some of it.
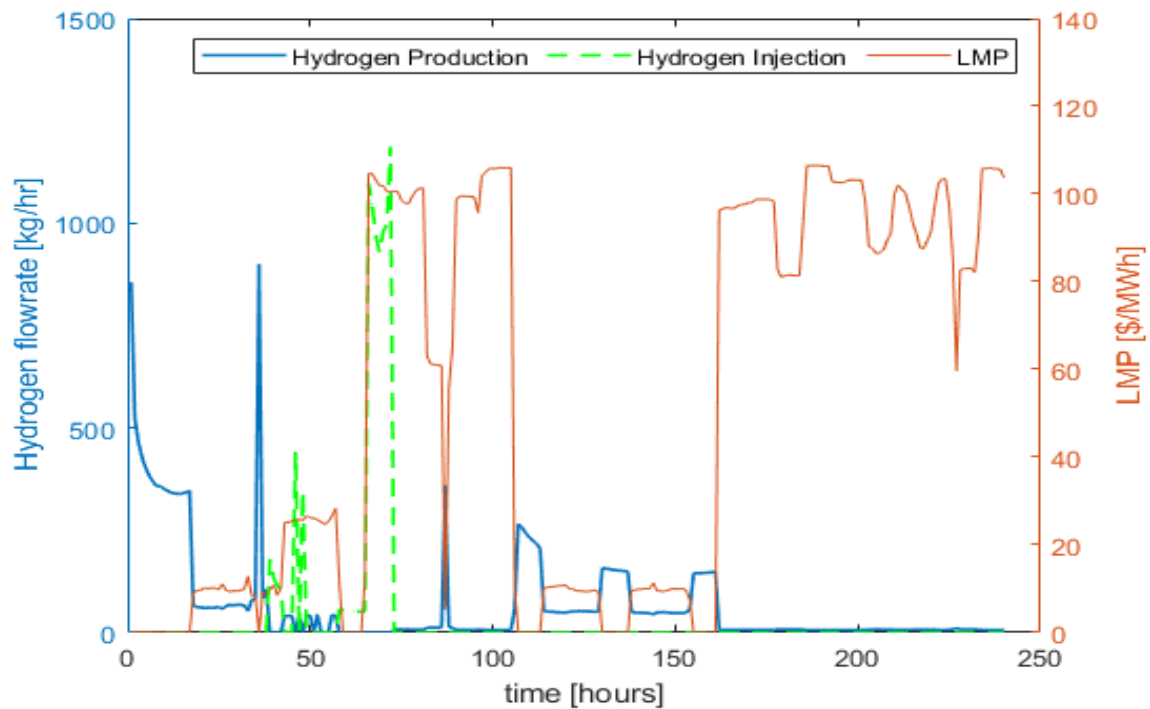
Figure 17. Hydrogen production and consumption trend**.**

The rate of CO_2 in the flue gas increases as the rate of natural gas utilization in the NGCC increases. That is when the LMP is high and the NGCC is producing power at close to maximum capacity, the rate of natural gas injection be high and subsequently the rate of CO_2 emission. However, the decision of whether to capture the CO_2 or not is affected by the value of the LMP at that hour. At a very high LMP, it may be profitable just to sell all the power produced to the grid and pay the tax penalty for releasing CO_2. Also, if the LMP is not high enough, it is profitable to use some of the power produced by the NGCC to power the PCC and the CO_2 compression train. So, in most cases the rate of CO_2 captured is 95%. Whenever, hydrogen is injected into the NGCC, the amount of the CO_2 in the flue always reduces, so in this case, CO_2 could be released rather than captured. The choice of whether to run the PCC and compressor train or pay the tax penalty is dependent on the amount CO_2 in flue gas and LMP. This profile can be observed in Figure 18.
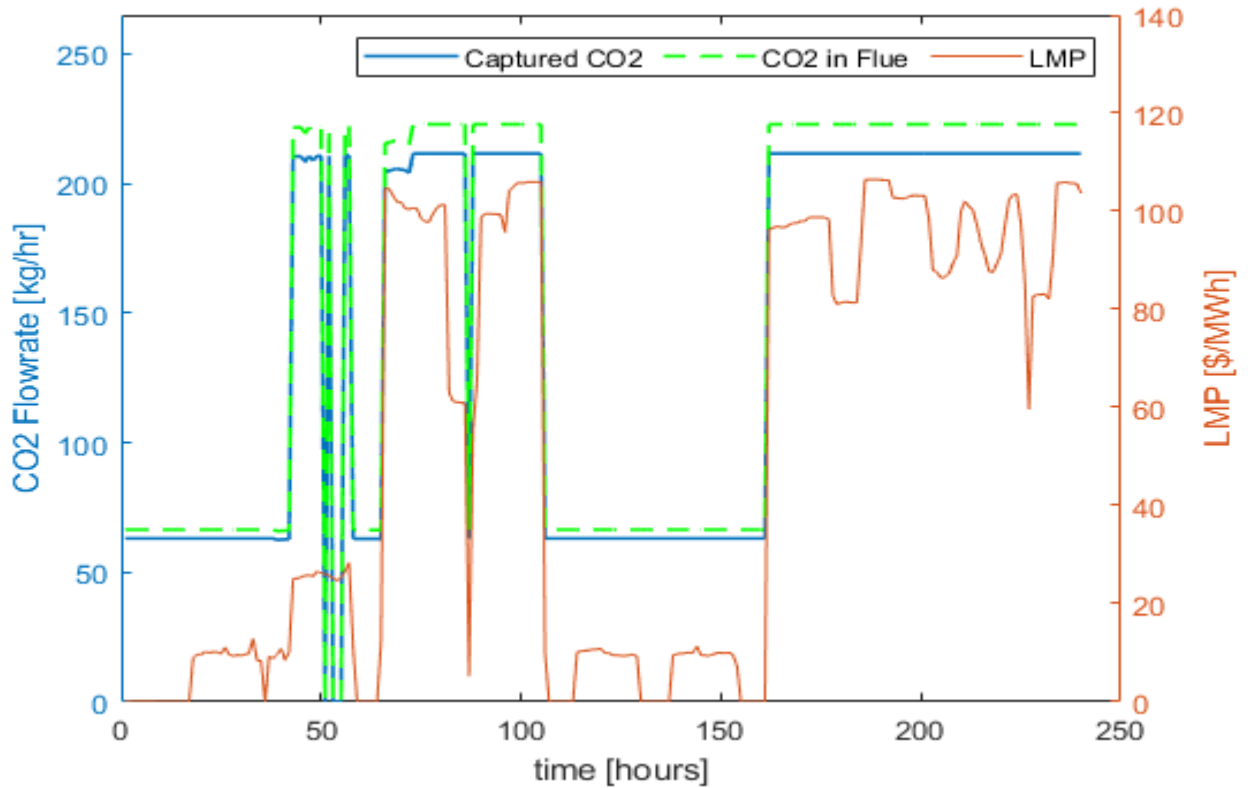
Figure 18. Trend of CO_2 released and captured.

The optimizer also placed an optimal value for the design capacity of components of the integrated plant. These values are shown in Table 18. The PCC can capture about 223 ton/hr of CO_2 and the volume of hydrogen storage required is about 1935 m^3. Lastly, the optimal design capacity of the PEM electrolyzer is 55 MW.

Table 21. Optimal design capacity

Design Variables	Optimum Value
PCC Capacity	222.91 ton/h
Hydrogen Storage Volume	1935.76 m^3
Maximum Electrolyzer Load	55MW

Also, the NPV, the capital expenditure and operating expenditures values are compared for both clustered and continuous cases. The difference in the NPV for a clustered case and a continuous case is about 4%, which is in the acceptable range. Also, the CAPEX, fixed OPEX and variable OPEX for both the clustered case and full case compared well and the difference between them is less than 0.5%. It takes about 3 hours for the clustered case to solve, and it takes about 8 hours for the continuous case to solve. This further shows the benefit of solving a clustered LMP profile rather than a continuous profile since the results compared well in both cases and clustered case solved much faster.
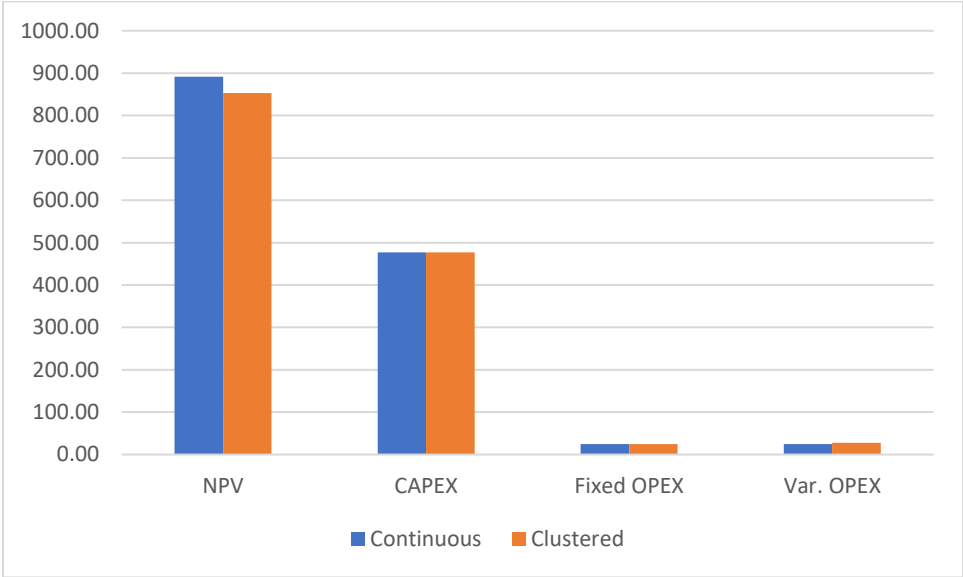
Figure 19. Comparison of NPV, CAPEX and OPEX for continuous and clustered LMP.

Chapter 4

Model Development, Validation and Optimization for Standalone H₂ Storage System to Utilize in the Peaker Plant

4.1 Hydrogen storage model development for standalone utilization in peaker plant (Objective#4)

This section will mainly focus on design optimization of cylindrical vessels. Another important consideration in our geometry consideration is the choice of vessel head. Even though various types of heads are available such as ellipsoidal, torispherical, hemispherical, conical, toriconical, etc., hemispherical head is often used when the design pressure is more than 500 psig.

4.1.1 Cylindrical Vessel

Compressed hydrogen gas is mostly stored using cylindrical vessel. Eqs. 65-80 are the design equations which are used for determining optimum vessel configuration. The hydrogen storage vessel was modeled in accordance with ASME BVP Section VIII Div-1 code. Minimum thickness required based on the circumferential stress and longitudinal stress are given by t_c and t_l, respectively. Minimum thickness is given by t_u. The maximum of these three thickness is usually considered as the required thickness to which corrosion allowance is added to obtain the final thickness as shown in Eq. 71.

Table 22. Design Equation of the Hydrogen Storage Vessel Shell

$$V_{H2} = \pi R^2 L \tag{65}$$

$$t_u = 1.5 \ mm$$

If $P \leq 0.385SE$

$$t_c = \frac{PR}{SE - 0.6P} \tag{66}$$

Else if $P > 0.385SE$

$$t_c = R\left(e^{\frac{P}{SE}} - 1\right) \tag{67}$$

If $P \leq 1.25SE$

$$t_l = \frac{PR}{2SE + 0.4P} \tag{68}$$

38

Table 22 Cont'd. Design Equation of the Hydrogen Storage Vessel Shell

Else if $P > 1.25SE$

$$t_l = R\left(\sqrt{\frac{P}{SE} + 1} \; - 1\right) \tag{69}$$

$$t = \text{maximum}(t_c, t_l, t_u) \tag{70}$$

$$t_d = t + corossion\ allowance \tag{71}$$

$$t_n > t_d \tag{72}$$

$$t_{nc} = t_n - corossion\ allowance \tag{73}$$

If $t \le R/2$

$$MAWP_c = \frac{SEt_{nc}}{R + 0.6t_{nc}} \tag{74}$$

Else if $t > R/2$

$$MAWP_c = SElog_e\left(\frac{R + t_{nc}}{R}\right) \tag{75}$$

If $t \le R/2$

$$MAWP_l = \frac{2SEt_{nc}}{R - 0.4t_{nc}} \tag{76}$$

Else if $t > R/2$

$$MAWP_l = SE\left(\left(\frac{R+t_{nc}}{R}\right)^2 - 1\right) \tag{77}$$

$$MAWP = minimum(MAWP_c, MAWP_l) \tag{78}$$

$$Vm = \pi L(Ro^2 - R^2) \tag{79}$$

$$R_o = t + R \tag{80}$$

The welding efficiency (E) and the allowable stress (S) are dependent on the material of construction of the vessel and the condition of storage. The maximum allowable pressure (MAWP) of the vessel is computed using the nominal thickness of the vessel. The nominal thickness must be greater than the design thickness of this vessel as shown in Eq. 82. Upon accounting for corrosion, the MAWP is estimated using Eq. 84-88. The minimum of the circumferential MAWP and longitudinal MAWP is used as the MAWP for the vessel. The thickness of the vessel is added

to the internal radius to estimate the external radius (Eq. 80). The volume of metal is calculated using Eq. 79. Equation 81 and 82 are used to estimate the thickness required for a hemispherical head. Eq. 83 or 84 is used for estimating MAWP. Eq. 85 is used to calculate the volume of the metal. The overall volume and mass of the metal are calculated using Eq. 86a and 86b respectively. In order to account for other materials needed for construction such as vessel supports, nozzles, mesh etc., a factor is added to calculate the gross weight as shown in Eq. 86c.

Table 23. Design Equation of the Hydrogen Storage Vessel Head

If $P \leq 0.665SE$

$$t = \frac{PR}{2SE - 0.2P} \tag{81}$$

Else if $P > 0.665SE$

$$t = R\left(e^{\frac{0.5P}{SE}} - 1\right) \tag{82}$$

If $t \leq 0.356R$

$$MAWP = \frac{2SEt_{nc}}{R - 0.4t_{nc}} \tag{83}$$

Else if $t > 0.356R$

$$MAWP = 2SElog_e\left(\frac{R + t_{nc}}{R}\right) \tag{84}$$

$$V_{mh} = \frac{2\pi(R_o^3 - R^3)}{3} \tag{85}$$

$$V_t = V_m + 2V_{mh} \tag{86a}$$

$$W = Density\ of\ Material * V_t \tag{86b}$$

$$W_{gross} = W\left(1 + \frac{F}{100}\right) \tag{86c}$$

4.1.2 Optimal Design and CAPEX of a Hydrogen Storage Vessel: A Test Case Scenario

Equations needed for cost calculations are shown in Eq. 87-95. Two of the most popular approach in the literature is the Lang factor approach and the module factor approach. The Lang factor approach is shown in Eq. 88. For fluid processing plant, the lang factor is 4.74, which can be used for H_2 storage vessels. But the module factor approach is considered in this study because Lang factor is often when an equipment has already being purchased (when the cost of the equipment is already known) while the bare module approach can also estimate the cost of the equipment. The bare module cost is given by Eq. 89. The total module cost is given by Eq. 90. Eqs. 91-95 represent additional terms including those used for considering the material of construction and operating pressure.

Table 24. Capital Cost Equation of Hydrogen Storage Vessel

$$C_{p,veseel} = C_p^o \, F_p F_M \tag{87}$$

$$C_{TM} = F_{lang} \sum C_{p,vessel} \tag{88}$$

$$C_{BM} = C_p^o \, F_{BM} \tag{89}$$

$$C_{TM} = 1.18 \sum C_{BM} \tag{90}$$

$$\log_{10} C_p^o = K_1 + K_2 \log_{10} A + K_3 \, (\log_{10} A)^{\wedge}2 \tag{91}$$

$$F_{P,Vessel} = 1 \quad \text{for} \quad t_{vessel} < t_{min} \text{ and } P > -0.5 barg \tag{92}$$

$$F_{P,Vessel} = \frac{\frac{(P+1)D}{2[850-0.6(P+1)]}+0.00315}{0.0063} \quad \text{for } t_{vessel} > t_{min} \text{ and } P > -0.5 barg \tag{93}$$

$$F_{P,Vessel} = 1.25 \quad \text{for} \quad P < -0.5 barg \tag{94}$$

$$F_{BM} = B_1 + B_2 F_p F_M \tag{95}$$

4.1.3 Test case CAPEX optimization of a cylindrical hydrogen storage

Here, we have run a test case for CAPEX optimization of a cylindrical hydrogen storage. For that we are considering is to store a 6000 kg of hydrogen gas at 303 K. The objective function is given by Eq. 96 and the gas equation for real gas is used here as given by Eq. 97. The cost factors for horizontal and vertical cylindrical vessel for the developed cost model are given in Table 4A, Appendix IV. The optimization result is provided in Table 20.

$$min\ C_{TM} \tag{96}$$

$$V_{H2} = \frac{Zm_{H2}RT}{P_{H2}M_{H2}} \tag{97}$$

With the inclusion of equation 97 as a constraint, the optimizer was able to adequately find the tradeoff between an increasing pressure compared to volume. From the costing equation, the volume of vessel is used to compute the cost of the vessel, so we expect the optimizer to settle for a low volume. But, as volume decreases, pressure increases and so is the required vessel thickness and the pressure factor. Essentially, this optimization helps us get an optimal value for all these parameters.

Table 25. CAPEX Comparison of the Optimal Design

Parameters	Optimum Value
Volume of Hydrogen, m^3	1269.78
Pressure of Hydrogen, Bar	62.00
Volume of Vessel, m^3	281.56
Design Pressure of Vessel, Bar	62.00
CAPEX of storage vessel, $MM	3.21

For the test case, in order to store a 6000 kg of hydrogen, a vessel with design volume of 281.56 m^3 and pressure of 62.00 bar is required. The volume and pressure of hydrogen being stored at this condition is 1270 m^3 and 62 bar respectively. Also, the capital cost of this vessel is \$3.21M. This value results to about 535/kg H_2 which is little higher than the quotation of global manufacturer of \$500/kg-H_2 and a lot less than the quote of US manufacturer of \$1000/kg H_2 for a vessel of similar design pressure.

4.2 NPV Optimization of Peaker Plant with Design and Operation of Hydrogen Production using Alkaline Electrolyzer (Objective#5)

In this work, we aim to optimally design a gas turbine that utilizes hydrogen generated from an alkaline electrolyzer and stored in a compressed hydrogen vessel. The optimal design of the vessel and the optimal operation of the electrolyzer and the gas turbine is considered as Peaker Plant and will be investigated in this work. The optimal design and set up of the hydrogen storage model for a cylindrical vessel has been done in the previous section. So, we will focus on developing a data driven model based on a high-fidelity model from the literature for the alkaline electrolyzer and the gas turbine. Finally, an NPV optimization is performed for the developed model for Peaker plant by utilizing clustered LMP.

4.2.1 Alkaline Water Electrolyzer

A high-fidelity Aspen Plus model of an alkaline electrolyser was developed by Monica et al [23]. The model was a hybrid of empirical model developed in ACM and unit operation models in Aspen Plus (Figure 20). Faradaic efficiencies and the coefficients of the polarization curve and gas purity used for building the empirical model has earlier been validated with experimental data by the authors. The model included the balance of plant for the complete generation of hydrogen using alkaline electrolyzer. In the model, it was assumed that all processes operate at a steady state. An ideal gas behavior is assumed for the gases. Deionized water is fed into the system at 25°C, and the hydrogen and oxygen output are obtained at 25°C. The alkaline electrolyzer is operated at balanced anode and cathode pressure. Effects of temperature and current density on the stack performance was investigated as shown in Figures 4A and 4B in APPENDIX IV. Figure 4B (a-c) in APPENDIX IV show the effect of pressure and current density on stack performance and hydrogen production rate at 75°C. The efficiency and specific power consumption with respect to

current density are also plotted as shown in Figure 21. The data available form this reference will is used to develop a data-driven model of the electrolyzer.
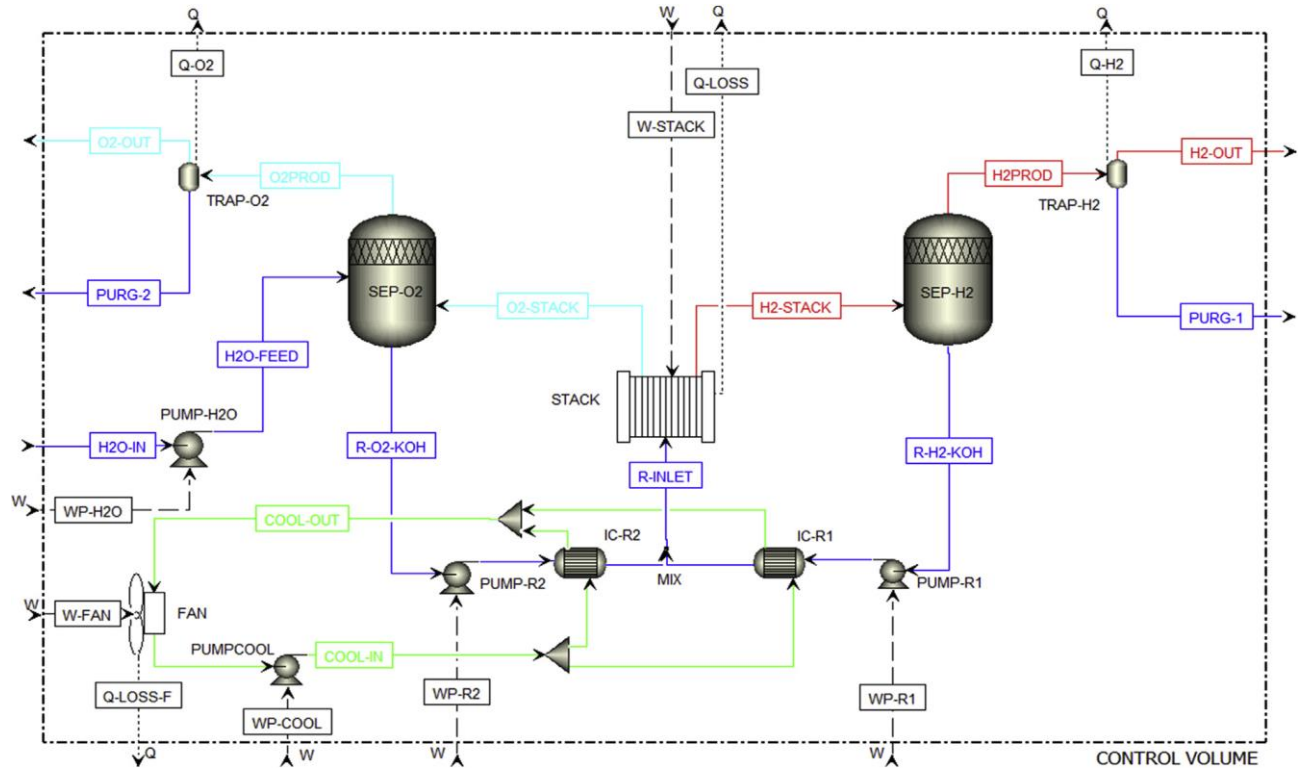

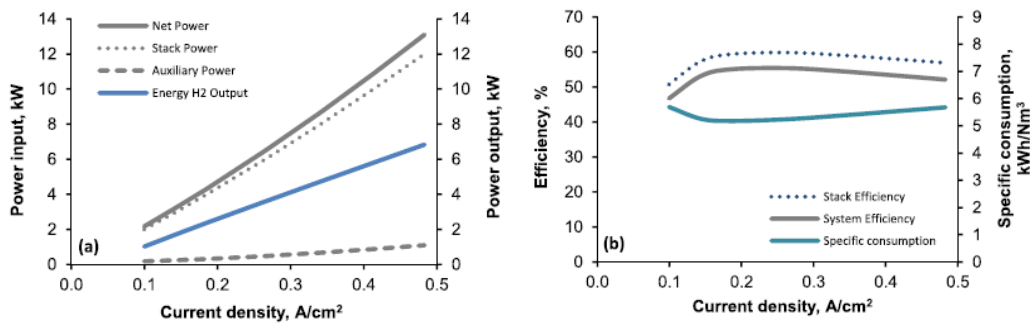**Figure 20.** Aspen Plus process flow diagram of an alkaline electrolysis plant [23]

Figure 21. Power and Efficiency plot with respect to current density for the alkaline water electrolyzer, (a) Stack power, net power and auxiliary power and power output, (b) Stack and system energy efficiencies and specific power consumption [23].

From the relationship above and figure 4B in APPENDIX IV, we can easily deduce that there is a linear relationship between current density and hydrogen flowrate. As the current density increases, the hydrogen flowrate increases. Our main aim is to find the relationship between hydrogen production rate and power specific power consumption of the electrolyzer. We therefore explore the result provided from the aspen model showing the relationship between the specific consumption and current density. Figure 21 shows the relationship between current density and system efficiency and specific consumption. We extracted the data for the specific consumption to model the relationship between hydrogen production rate and specific consumption.

4.2.2 Data Driven Alkaline Water Electrolyzer Model

Electrolyzer utilization (EU) can be represented by Eq. 98, i.e., in terms of relative current density or, equivalently, in terms of H_2 production rate as shown in Eq. 99.

$$EU = \frac{Current\ Density_i}{Max\ Current\ Density} \tag{98}$$

$$EU = \frac{Hydrogen\ Producdtion\ rate_i}{Max\ Hydrogen\ Production\ rate} \tag{99}$$

Also, we converted the specific consumption from $\frac{kWh}{Nm^3}$ to $\frac{kWh}{kg}$ because of convenience. Figure 22 shows the fit of a 3rd order polynomial model to the data [23]. This model is represented in Eqn 100, where SC represents the specific consumption in $\frac{kWh}{kg}$ and EU is the electrolyzer utilization defined by Eqn. 98 and 99.

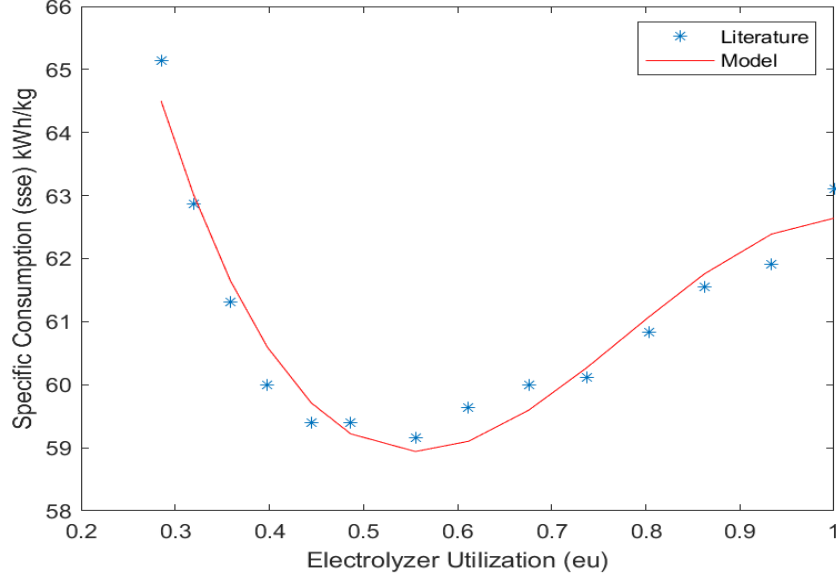$$SC = 89.54 - 135.17EU + 189.04EU^2 - 80.76EU^3 \tag{100}$$

Figure 22. Validation of the literature data [23] with our developed model.

4.2.3 Costing Model for The Alkaline Water Electrolyzer

Roberta et. al [63] analyzed the cost of generating hydrogen based on industrial data from multiple sources by using the Monte-Carlo approach. They divided the cost of production into low, mid, and high regime. In the current set-up, we use a value of $988/kW for the evaluation of the electrolyzer CAPEX. This value falls in the mid region of the capital cost study. In this work, the fixed operating and maintenance cost is specified to be $40/kW while the variable operating, and maintenance is 0.08$/kg of hydrogen produced.

Table 26. Costing Model for Alkaline Water Electrolyzer

$Electrolyzer_{CAPEX} = 988 * Capacity\ of\ the\ electrolyzer\ (kW)$	$101a$
$Electrolyzer_{fixed}OAM = 40 * Capacity\ of\ the\ electrolyzer\ (kW)$	$101b$
$Electrolyzer_{Var}OAM_h = 0.08 * H_2Flowrate_h$	$101c$

4.2.4 Aeroderivative Gas Turbine Model

A polynomial model was developed to capture the operational efficiency of the aeroderivative turbine. This model shows the operating relationship between the thermal efficiency and the power output of the LM2500 aeroderivative turbine [47,48]. This model helps us creates a

relationship that captures the amount of hydrogen injected into the gas turbine to produce a certain amount of power from the gas turbine.

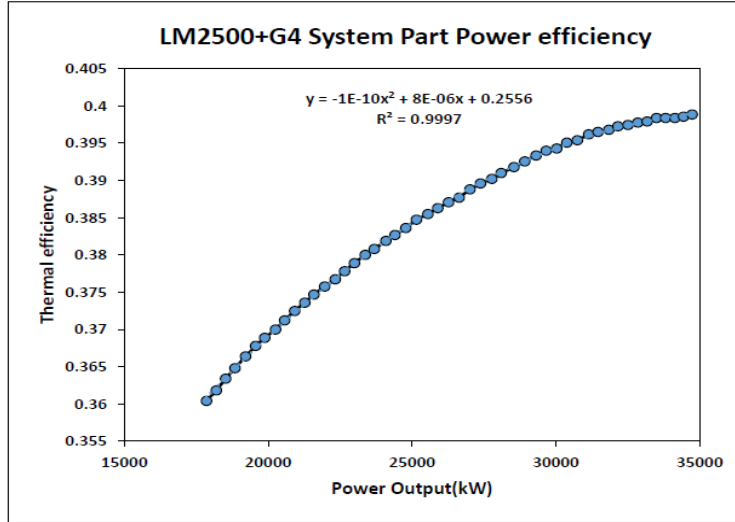$$Eff = 0.2556 + 8e^{-6}P_{output} - 1e^{-10}P^2_{output} \qquad (102)$$

Figure 23. LM2500 system operating efficiency [48].

The gas turbine fuel is assumed to be a mixture of hydrogen and natural gas. In this case the lower heating values of both hydrogen and natural gas is involved in the computation of the operational efficiency, power generation and fuel consumption. Just as with the case with 100% natural gas injection, we applied similar equations but here we also accounted for the presence of natural gas in the fuel mix. The volumetric percentage of the fuel is x, and this can be used to compute the injection rate of each of the fuel (H_2 and NG). The adjustment to this formulation is shown in the following equations. The costing equation to estimate the capital and the operating costs of the gas turbine is presented in Table 22.

Table 27. Aeroderivative Gas Turbine Model

$$Fuel\ injection\ rate_f \left(\frac{kg}{hr}\right) = x_f \rho_f V_T \tag{103}$$

$$\sum_{f \in H_2, NG} x_f = 100 \tag{104}$$

$$Thermal\ Efficiency = \frac{Work\ Output(Power\ produced)\ MW_e}{Heat\ Input\ MW_{th}} \tag{105}$$

$$Heat\ Input\ (MW_{th}) = \sum_{f \in H_2, NG} LHV_f * Fuel\ injection\ rate_f \tag{106}$$

The capital cost of the aeroderivative gas turbine is estimated at \$1000/kW power produced [65]. Also, the fixed OPEX of the gas turbine is a fraction of the CAPEX and the variable OPEX is a function of the power produced by the turbine at every point in time. For a sample fuel mix flow with 15% hydrogen volumetric composition, at 9 bar and 298K, the volumetric flowrate for the two fuel is plotted against the power generation. This is shown in Figure 24.

Table 28. Costing Model for Aeroderivative Gas Turbine [64,65]

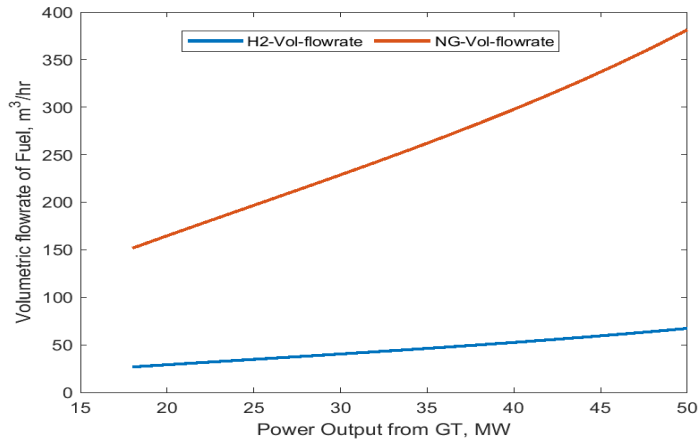|	
$GT_{CAPEX} = 1000 * Capacity_{GT}$	$(107a)$
$GT_{fixed\ OPEX} = 0.0153 * GT_{CAPEX}$	$(107b)$
$GT_{var\ OPEX} = 0.695 * P_{GT}$	$(107c)$

Figure 24. Fuel volumetric flowrate plot for the gas turbine.

4.3 NPV Optimization Set-Up for Integrated Peaker Plant

The net present value of the hydrogen utilization gas turbine integrated with hydrogen production is optimally computed putting into account all the constraints imposed by the operational models of the units that made up the plant. The optimization scheme is shown in Figure 25. The operational models enable us to compute the variable operational expenditure of the plant's units, and this is a function of either the hydrogen produced for the electrolyzer, or the power generated for the gas turbine. The objective function (Table 23, Eqn 108) being optimized in this case is the NPV of the plant. The assumed interest rate is 7.25% and the plant expected year of operation is 30 years. These parameters are used to calculate the present annuity factor that we eventually used to scale down the capital expenditure to hourly rate.
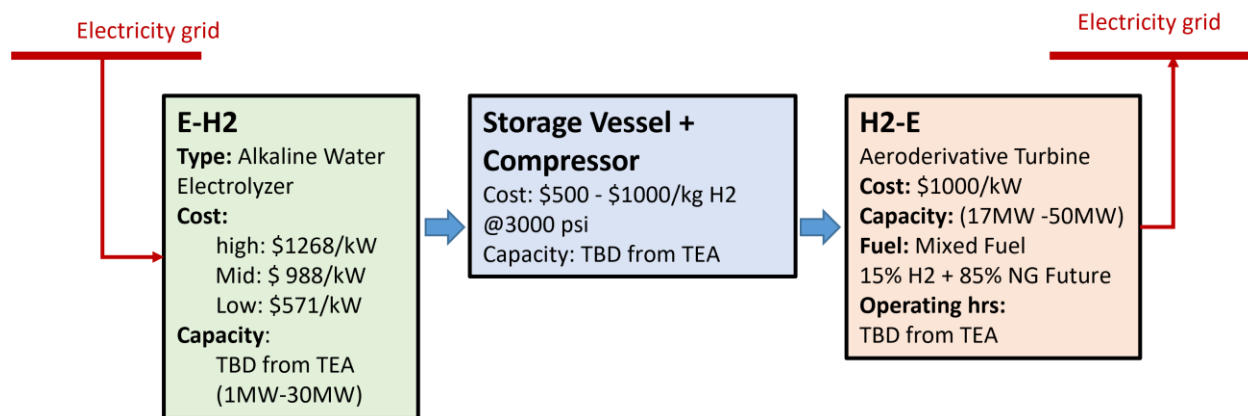

Figure 25. Flowsheet of the optimization scheme.

Table 29. Objective Function of the Integrated Peaker Plant

$$\max NPV = P_{A,f} \sum_{t=1}^{8760} REVENUE_t - CAPEX - P_{A,f} OPEX_{fixed} \tag{108}$$

$$REVENUE_t = LMP_t P_{grid,t} - LMP_t P_{consumed,t} - OPEX_{variable,t} \tag{109}$$

$$P_{grid,t} = GT\ power\ produced$$

$$P_{consumed,t} = Electrolyzer\ Power\ + H_2\ Compressor\ power + H_2\ Expander\ power \tag{110}$$

$$P_{A,f} = \frac{(1+i)^n - 1}{i(1+i)^n} \cdot \frac{1}{(1+i)^n} \tag{111}$$

$$\forall\, t \in T$$

The constraints involved in the optimization are the operating models of the alkaline water electrolyzer, hydrogen compressors and coolers, and the aeroderivative gas turbine. Another important constraint that we add to ensure that the operation of the electrolyzer and the gas turbine is mutually exclusive is shown in the equation below.

$$H_2\ Injection\ rate * H_2\ Production\ rate < 0.001 \tag{112}$$

4.3.1 Problem Formulation

We are currently looking at four different scenarios to understand the operational profitability of the gas turbine subjected to the composition of hydrogen gas in the NG-H_2 mixed fuel. Also, we will assess the impact of the tax paid on CO_2 released due to the usage of natural gas in the gas turbine. The Table 24 below shows the four cases and their brief definition.

Table 30. Cases for Plant Configuration

	Case 1	Case 2	Case 3	Case 4
CO_2 Tax ($/ton)	100	100	0	0
H_2 as Fuel (Vol%)	15%	0-15%	15%	0-15%

In case 1, it is assumed that a tax of $100/ton of CO_2 released and the 15% hydrogen by volume is used in NG-H_2 fuel mix. This case restricts the composition of the fuel mix in the turbine to 85% natural gas and 15% hydrogen by volume. This composition scenario is the same for case 3. But

in case 3, we assumed that there is no penalty for CO_2 released. This means that the CO_2 tax for that case is \$0/ton of CO_2 emitted. Case 2 has the same tax penalty as case 1 but in case 2, the percentage volume of hydrogen in the fuel mix varies from around 0 to 15%. This gives us the opportunity to see if it's optimal or more profitable to run the plant at a lower hydrogen present by volume. Case 2 and Case 4 both has this hydrogen percentage variation but case 4 like case 3 has no CO_2 tax penalty. Most of the constraints are linear and the nonlinear constraints are polynomial constraints to degree 3 in some cases. So, feasibility is not a challenge here but the instability in the LMP causing convergence to take quite some time.

4.3.2 Optimization Results and Discussions

Design Capacity of components of the plant

The electrolyzer load for Case 2 and Case 4 is low at 1MW. The fuel mix does not have 15% hydrogen utilization constraint. The average utilization of hydrogen in these two cases are less than 1%. As a result, the design capacity of the hydrogen storage vessel in these cases are lower. A vessel with design pressure of 90 bar will be sufficient for case 2. In Case 4, even though a 1MW electrolyzer is available, it is not being utilized as hydrogen was not produced thought out the run. For that reason, no hydrogen storage vessel is required for Case 4.

Table 31. Optimal Design Capacities for Plant Components

Variables	Case 1	Case 2	Case 3	Case 4
Electrolyser Design Load, MW	4.50	1	20.22	1
H_2 Storage Volume, m^3	409.38	171.5	179.68	0
H_2 Storage Vessel Pressure, bar	96.15	90.00	219.08	-
Max Mass of Hydrogen, kg	3000.00	1510.00	3000.00	-
GT Design Load, MW	33.25	50.00	50.00	50.00
GT capacity factor	0.27	0.50	0.51	0.66
Average GT power, MW	9.09	24.91	25.71	32.97

The electrolyzer design capacity for Case 3 is the highest followed by that of Case 1. One might expect Case 1 to produce more hydrogen and utilize more hydrogen because of the carbon tax penalty, but in Case 1 the GT capacity, Average GT power and utilization are lower than Case 3.

The design pressure of the storage vessel is also high for Case 3 with Case 3 having the highest design pressure. This is expected since more hydrogen is being produced in this case. We consider case 4 (no CO_2 tax and percentage H_2 Vol 0-15%) to understand the hydrogen economy in the integrated plant. We want to know if the CO2 tax incentive is enough to enable the profitable production and utilization of hydrogen in the set up. In case 2, where there is CO2 tax, the plant utilizes the 1MW electrolyzer to supplement the NG in the fuel mix, but this is only to reduce the CO2 tax penalty paid. In case 4, even though this 1MW electrolyzer is present as a necessary investment, it is not utilized still because the tax incentive is not enough to offset the deficit from hydrogen production.

NPV for the cases under consideration

The NPV for the four different cases are shown in Figure 26. Case 4 has the highest NPV for the LMP being considered. Case 3 & 4 are expected of course to have a high NPV because of the zero-carbon tax scenario. Case 2 has a very high NPV compared to Case 1 because of the hydrogen utilization of 15% by volume placed on the gas turbine fuel mix in Case 1. This means that paying the tax penalty and utilizing more natural gas than the 85% natural gas condition in Case 1 is much more profitable. As a result, the hydrogen volumetric utilization varies in Case 2 & 4. The NPV in Case 4 is also greater than that of case 3 because of the same reason. Even though both cases assume a zero tax.
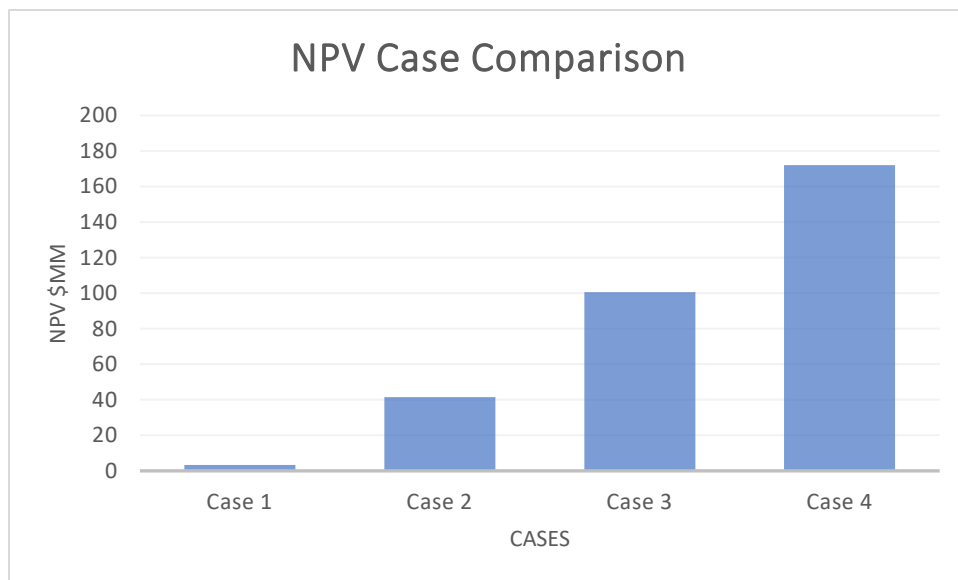

Figure 26. NPV Comparison for the four cases.

The capital cost for the gas turbine is the highest for all the cases. However, the capital cost for electrolyzer is high for only Case 1 & 3. This is because of the need to produce enough hydrogen to meet up with the 15% hydrogen by volume whenever the gas turbine is running.
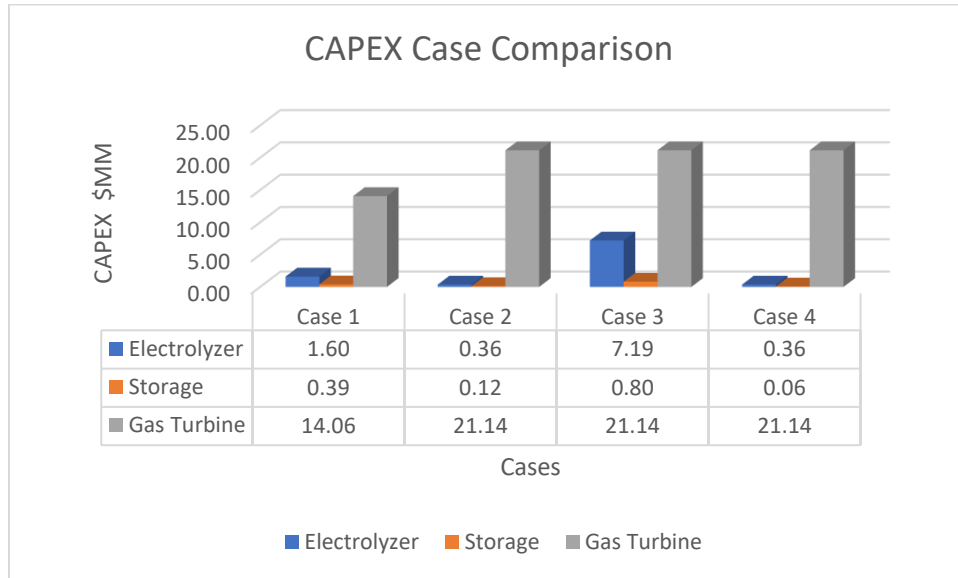

Figure 27. CAPEX Comparison for the four cases.

As a result of hydrogen production rate been higher in Case 1 and 3, the capital cost of the hydrogen storage vessel and compressor system is also relatively higher when compared Case 2 and Case 4. The assumption here is that an electrolyzer must be part of the investment and the minimum capacity of the electrolyzer considered is 1MW. If the lower bound of the electrolyzer capacity is set to 0, both case 2 & case 4 yield the same result. But we intend to understand the dynamics hydrogen brings into the economic configuration, that is why we mandated a small size electrolyzer. The NPV for case 2 is $3.71MM and that of case 4 is $15.40 despite case 4 paying about $1.2MM for the electrolyzer and not utilizing it.
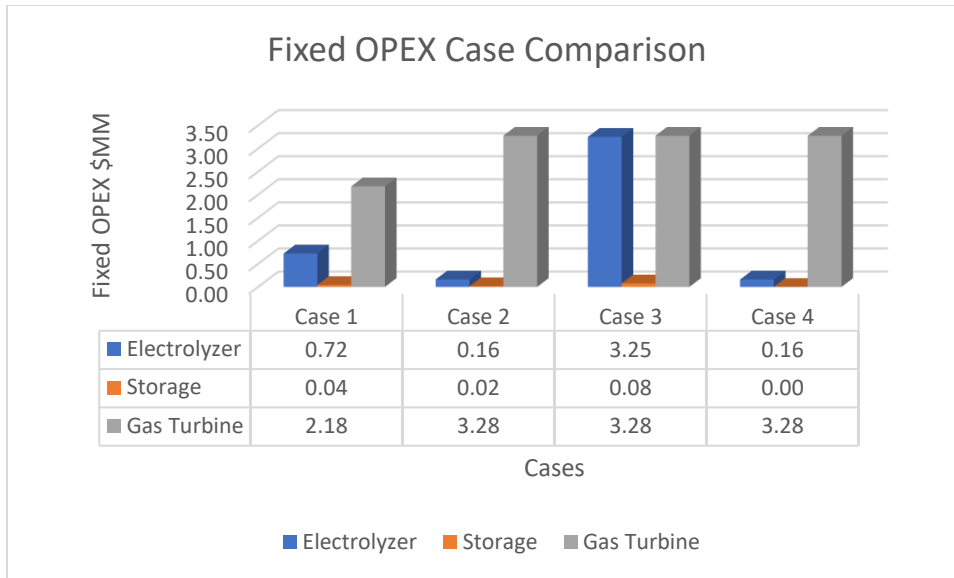
Figure 28. Fixed OPEX Comparison for the four cases.

The fixed operational and maintenance cost is high for the alkaline water electrolyzer, and this value is reflected in Case 1 & 3. Compared to the capital cost, the fixed OPEX of the electrolyzer is relatively well pronounced when compared to capital cost.
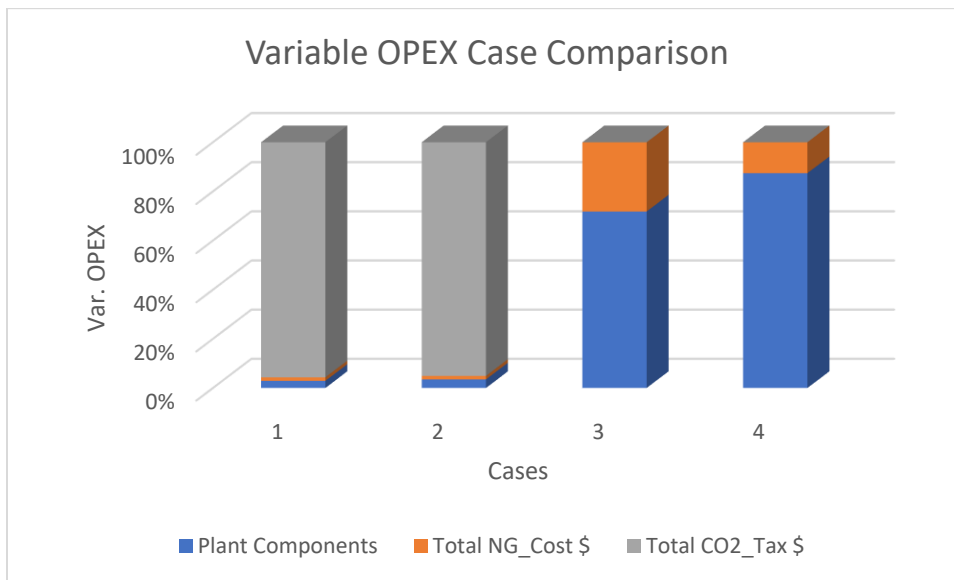

Figure 29. Variable Expenditure comparison for the four cases.

Figure 29 showing the composition by percentage of the variable expenditures in the plant. The carbon tax is playing a major role in the total variable operating expenditure, and this is having

a huge impact on the operation of the plant. This high carbon tax will make it impossible to run the plants at some average LMP that are not high enough to offset the deficit this high carbon tax will introduce. Also, hydrogen utilization is a panacea to this, but majority of the fuel in the fuel mix is natural gas, meaning that the minimum amount of natural gas that we can have in the fuel mix is 85% by volume, that is a lot of percentage by mass because of the low volumetric density of energy. In case 3 &4 where there is no carbon tax, the variable OPEX of the plants components is playing the major role as expected.

Steady-State results and transient profile

The GT produces power near its maximum capacity at high LMP and shut down at low LMP. This is the expected scenario for the four cases. Figure 30 a-c represents some notable trends for Case 1. Cases 1 and 3 are similar because of the 15% composition of hydrogen.
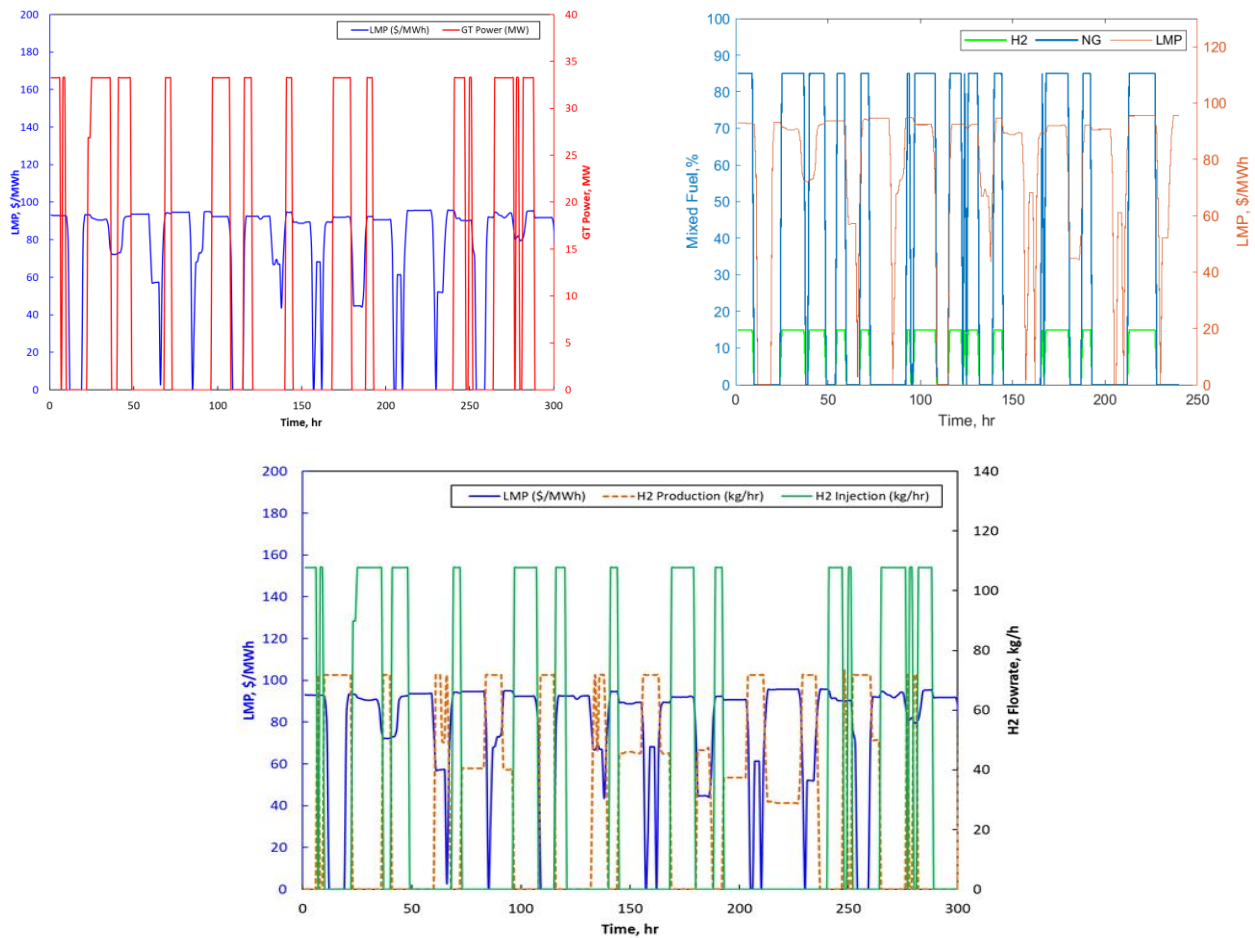

Figure 30. Power and hydrogen flowrate profile for 10 days period for Case 1 a. Gross power GT power trend b. Fuel composition trend c. Hydrogen flowrate trend.

At low LMP, the electrolyzer produces hydrogen. This is because the cost of buying power from the grid is low or even zero at low LMP and this boosts the NPV of the plant. The model profile of Case 1 is similar to Case 3. The profile for Case 3 can be seen is Figure 4C of APPENDIX IV. The only major difference is in the GT power production which gets up to 50MW for Case 3 but is only up to about 33MW for Case 1.

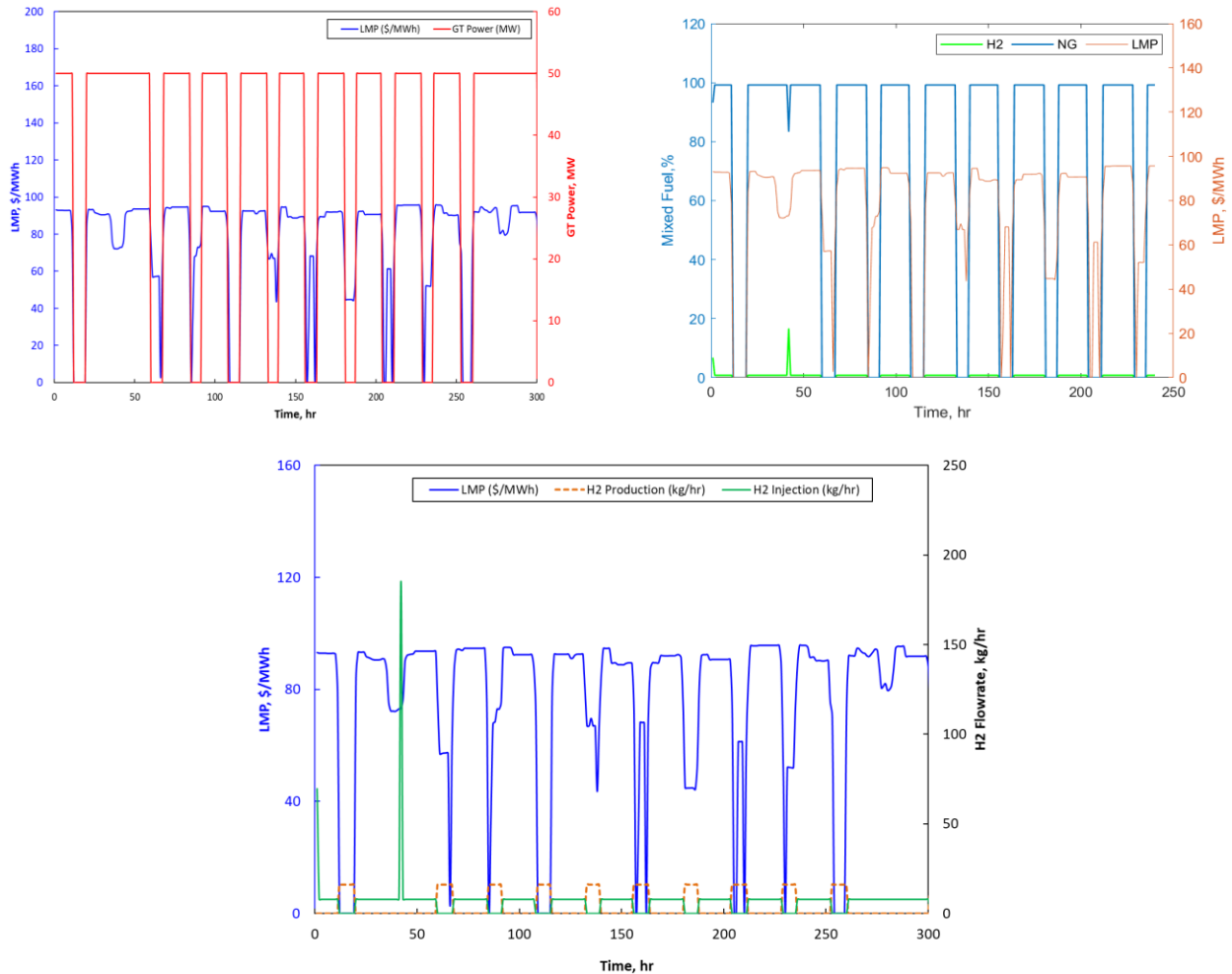**Figure 31.** Power and hydrogen flowrate profile for 10 days period for Case2 a. Gross power GT power trend b. Fuel composition trend c. Hydrogen flowrate trend.

Also, for Case 2, the power production gets to a maximum of 50MW when the LMP is high, and the GT shut down when the LMP is low. The hydrogen percentage composition here is below 1% in all cases as we can see in Figure 31b. Even though the rate of hydrogen utilization is

56

low in this case, the hydrogen production still happens at low LMP to supplement the natural gas being utilized in the GT turbine. Case 2 profile is similar to Case 4. The profiles for case 4 are presented in figure 1b Appendix 5. The rate of injection of hydrogen in Case 1 is around 71.86kg/hr. compared to 15.86kg/hr. in Case 2. This further explains why the capacity of the electrolyzer in Case 1 is higher than that of Case 2. Similarly, for Case 3, the hydrogen production and injection are lot higher that of Case 4.

Chapter 5

Conclusions and Future Recommendations

5.1 Conclusion

In this work, robust NPV optimizations were done to access the techno-economic feasibility of two different hydrogen utilization technologies. Due to the large non-linearity and the large data point involved in the yearlong optimization, a reduced order model was developed for some components of the plant. Also, a clustering algorithm was developed for the LMP profile of different electricity markets to reduce days needed for the optimization. Lastly, data-driven models were also developed to model the operational efficiency of some other component of the models.

In this study, the optimization of an NGCC power plant with carbon capture and H_2 storage systems was presented for a selected electricity market (PJM). The economics and feasibility of the PCC plant and H_2 production were investigated for this LMP profile. It was found that the addition of the PCC and electrolyzer units was economically favorable compared with a single NGCC plant and reduced the CO_2 emissions significantly. The optimal value for the PCC capacity ids found to be 222.91ton/h while the design load of the electrolyzer and the design hydrogen storage volume are 55MW and 1935.76m^3 respectively. The NPV optimization model was also able to predict the operation of the components of the integrated plant. Also, the optimal NPV of the plant for a 30-year operational period was found to be around $890M.

Another case of hydrogen production and utilization of an integrated system including electrolyzer, H_2 storage and aeroderivative turbine (GT) is developed in the Python platform for NPV optimization. The present work assumed that electricity consumed in the process is being purchased from the grid and produced electricity is sold to the grid and both are given by the LMP at that time instant. The current model is using a clustered LMP of California, where no of equivalent days are 131. Four case studies are being considered with CO_2 tax and H_2 volume percentage in the mixed fuel. The electrolyzer produces H_2 at low LMP and injected at high LMP. The max capacity of the turbine is 50 MW for Cases 2, 3 and 4, while it is about 33 MW for case 1. The NPV for Case 4 is the highest because of no carbon tax and the flexibility of hydrogen usage. For Case 4, even though a small electrolyzer of 1 MW is forced (minimum), it was not

optimal to use it; on the other hand, even though the electrolyzer design capacity is still at minimum for Case 2 like Case 4, electrolyzer was utilized to reduce the penalty from CO_2 tax.

5.2 Future Recommendations

In this course of study, the primary focus was to develop an optimization model to investigate the economic and operational feasibility of the hydrogen utilization in power plants with or without carbon capture technology. We can however do more sensitivity studies based on this current configuration and try out other configurations.

It is therefore recommended that the following studies should be done in the future.

- To better understand and have a more general understanding of the optimization models of the two configurations, it's important to carry out a sensitivity study for LMP of different electricity markets.
- Also, since a PEM electrolyzer is used in a configuration with carbon capture and alkaline electrolyzer is used in the Peaker plant configuration, a study should be carried out to determine if it's more profitable to swap the type electrolyzers used in the two configurations.
- A CAPEX based sensitivity study can be used to improve the techno-economic performance of the integration of hydrogen technology with power plants. The cost of hydrogen production has been projected to reduce as more improvement is made in renewable energy generation. This could open the potential opportunity for investing in a much cheaper hydrogen production alternative in the future. This potential technological improvement in hydrogen production should be accounted for in future work.
- The percentage of hydrogen utilization in the aeroderivative gas turbine needs to be increased in future study. As the need to radically reduce carbon emission globally emerges, utilization of more hydrogen in the gas turbine must be accomplished. The goal is to reach 100% H_2 utilization and this scenario needs to be investigated in future works.
- The flexibility of Peaker plants means they can operate only at hours of high-power demand. This situation often imposes a daily operating hour constraint on the aeroderivative turbine. This scenario needs to be included and investigated in future works.

References

1. Atika, Q., Fayaz, H., Narudin, A., Glenn H., Daniyal, A., Khaled, S., & Khalid, H. Towards sustainable energy: A systematic review of renewable energy sources, technologies, and public opinions. *IEEE* . (2019).

2. Enviromental and Energy Study Institute (EESI). https://www.eesi.org/topics/fossil-fuels/description#:~:text=Fossil%20fuels%E2%80%94including%20coal%2C%20oil,percent%20of%20the%20world's%20energy

3. National Oceanic and Atmospheric Administration (NOAA). https://www.esrl.noaa.gov/gmd/ccgg/trends/gl_trend.html. (2022).

4. Yan, Y., Tohid, N., Sai G., Kasturi, N., Vinlay, P., Arvind, R., Paula, N., Jude, O., Zhien Z., Ding, S., Lijuan, W., Wenbiao, Z., Yong, Y., William, A., Junyu, Y., Meihong, W., Edward, J., Vasilije, M., & Peter, T. Harnessing the power of machine learning for carbon capture, utilisation, and storage (CCUS) – a state-of-the-art review. *Energy Environ. Sci.* **14**, 6122–6157 (2021).

5. Nugroho, A. P., Kenshi, I., & Atsushi. K. Impact of hydrogen fuel for CO2 emission reduction in power generation sector in Japan Energy Procedia 105 (2017) 3075 – 3082.

6. Bernad C.T. & Somtochukwu G. N. Hydrogen Production, Distribution, Storage and Power Conversion in a Hydrogen Economy - A Technology Review. Chemical Engineering Journal Advances 8 (2021) 100172.

7. Office of Energy Efficiency & Renewable Energy. https://www.energy.gov/eere/fuelcells/hydrogen-storage (accessed on November 1, 2022)

8. Onboard Type IV Compressed Hydrogen Storage System- Cost and Performance Status 2015. DOE Hydrogen and Fuel Cells Program Record.

9. K. Mazloomi, C. Gomes, Hydrogen as an energy carrier: Prospects and Challenges, Renewable and Sustainable Energy Reviews 16 (5) (2012) 3024–3033.

10. International Energy Agency (IEA) The Future of Hydrogen Report https://www.iea.org/reports/the-future-of-hydrogen (accessed on November 1, 2022).

11. Granovskii M, Dincer I, Rosen MA. Exergetic life cycle assessment of hydrogen. production from renewables. J Power Sources 2007;167:461.

12. Charvin P., Stephane A., Florent L., & Gilles F. Analysis of solar chemical processes for hydrogen production from water splitting thermochemical cycles. Energy Conver Manage 2008;49:1547.

13. Sigurvinsson J., Mansilla C., Arnason B., Bontemps A., Marechal A., & Sigfusson T. Heat transfer problems for the production of hydrogen from geothermal energy.

14. Kothari R, Buddhi D, Sawhney RL. Sources and technology for hydrogen production: a review. Int J Global Energy Issues 2004;21:154.

15. Kewei H., Jiakun F., Xiaomeng A., Danji H., Zhiyao Z., Xiaobo Y., Comparative study of alkaline water electrolysis, proton exchange membrane water electrolysis and solid oxide electrolysis through multiphysics modelling. Applied Energy 312 (2022) 118788

16. Alfredo Ursu, Luis Marroyo, Eugenio Gubı, Luis M. Gandı, Pedro M. Dieguez, & Pablo Sanchis Influence of the power supply on the energy efficiency of an alkaline water electrolyser. International Journal of Hydrogen Energy 34 (2009) 3221-3233

17. Sinisa Z., Ivan Z., & Marko V. Evaluation of DC-DC resonant converters for solar hydrogen production based on load current characteristics. Research gate net publications 263470190

18. Yujing Guo, Gendi Li, Junbo Zhou and Yong Liu. Comparison between hydrogen production by alkaline water electrolysis and hydrogen production by PEM electrolysis. IOP Conf. Series: Earth and Environmental Science **371** (2019) 042022

19. Zeng K, Zhang D. Recent progress in alkaline water electrolysis for hydrogen production and applications. Prog Energy Combust Sci 2010;36:30726 https://doi.org/10.1016/j.pecs.2009.11.002.

20. CarmoM, FritzDL,Mergel J, Stolten D. A comprehensive review on PEM water electrolysis. Int J Hydrogen Energy 2013;38:4901e34. https://doi.org/10.1016/j.ijhydene.2013.01.151.

21. Jorn B. & Thomas T. Alkaline Water Electrolysis Powered by Renewable Energy: A Review. Processes **2020**, 8, 248

22. Georgios S., Alejandro I., Vesa R., Antti K., Jero A., Olli B. Dynamic energy and mass balance model for an industrial alkaline water electrolyzer plant process. International Journal of Hydrogen Energy 47 (2022) 4328-4345

23. Monica S. Ernesto A., David A., Lourdes R., Carmen C. Aspen Plus model of an alkaline electrolysis system for hydrogen production. International Journal of Hydrogen Energy 45 (2020) 3916-3929

24. Janusz Kotowicz, Michał Jurczyk_, Daniel We̢cel, Włodzimierz Ogulewicz. Analysis of Hydrogen Production in Alkaline Electrolyzers. Journal of Power Technologies 96 (3) (2016) 149-156

25. Jonathon Y., Rahman D., Robert P., Renate E., Rose A., Anita Ho-Baille, and Nathan L. Techno-economic Analysis of Hydrogen Electrolysis from Off-Grid Stand-Alone Photovoltaic Incorporating Uncertainty Analysis. Cell Reports Physical Science 1, 100209

26. Green Hydrogen Cost Reduction. International Journal of Renewable Energy Agency (IRENA)

27. Hydrogen Production Cost from PEM Electrolysis. DOE Hydrogen and Fuel Cells Program Record.

28. Sayed M. Saba, Martin Muller, Martin Robinius, Detlef Stolten. The investment costs of electrolysis - Acomparison of cost studies from the past 30 years. International Journal of Hydrogen Energy 43 (2018) 1209-1223.

29. George B. and Andrew S. The Key Techno-Economic and Manufacturing Drivers for Reducing the Cost of Power-to-Gas and a Hydrogen-Enabled Energy System. **2021**, 2, 273–300. https://doi.org/10.3390/hydrogen2030015

30. Assessment of Hydrogen Production Costs from Electrolysis: United States and Europe. Adam Christensen.

31. Office of Energy Efficiency & Renewable Energy. https://www.energy.gov/eere/fuelcells/hydrogen-storage (accessed on November 1, 2022)

32. Costs of Storing and Transporting Hydrogen. 1998. NREL/TP-570-25106.

33. M. Cai, et al. (2015), Testing, Modelling, and Evaluation of Innovative Hydrogen Storage System Designs, presented at the 2015 DOE Hydrogen Program Annual Merit Review Meeting, Washington, D.C.

34. Cheng, F., Patankar, N., Chakrabarti, S. & Jenkins, J. D. Modeling the operational flexibility of natural gas combined cycle power plants coupled with flexible carbon capture and storage via solvent storage and flexible regeneration. *Int. J. Greenh. Gas Con.* **118**, 103686 (2022).

35. Hammond, G. P. & Ondo Akwe, S. S. Thermodynamic and related analysis of natural gas combined cycle power plants with and without carbon sequestration. *Int. J. Energy Res.* **31**, 1180–1201 (2007).

36. Mores, P. L., Juan, I. M., Nicolas, J. S., Jose A. C., Miguel C. M., & Sergio F. M. Optimization of the design, operating conditions, and coupling configuration of combined cycle power plants and CO2 capture processes by minimizing the mitigation cost. *Chem. Eng. J.* **331**, 870–894 (2018).

37. Oh, S. Y. & Kim, J. K. Operational optimization for part-load performance of amine-based post-combustion CO2 capture processes. *Energy* **146**, 57–66 (2018).

38. Litzelman, S. J., Tuttman, M., Devarakonda, M., Lyubovsky, M. & Duthu, R. Flexible CCS technologies to reduce the cost of net-zero carbon electricity systems. in *15th International Conference on Greenhouse Gas Control Technologies, GHGT-15* (2021).

39. Zantye, M. S., Arora, A. & Hasan, M. M. F. Renewable-integrated flexible carbon capture: A synergistic path forward to clean energy future. *Energy Environ. Sci.* **14**, 3986–4008 (2021).

40. Yuan, M., Teichgraeber, H., Wilcox, J. & Brandt, A. R. Design and operations optimization of membrane-based flexible carbon capture. *Int. J. Greenh. Gas Con.* **84**, 154–163 (2019).

41. Oates, D. L., Versteeg, P., Hittinger, E. & Jaramillo, P. Profitability of CCS with flue gas bypass and solvent storage. *Int. J. Greenh. Gas Con.* **27**, 279–288 (2014).

42. Bandyopadhyay, R. & Patiño-Echeverri, D. Alternative energy storage for wind power: Coal plants with amine-based CCS. *Energy Procedia* **63**, 7337–7348 (2014).

43. Cloete, S. & Hirth, L. Flexible power and hydrogen production: Finding synergy between CCS and variable renewables. *Energy* **192**, 116671 (2020).

44. Cloete, S., Ruhnau, O. & Hirth, L. On capital utilization in the hydrogen economy: The quest to minimize idle capacity in renewables-rich energy systems. *Int. J. Hydrogen Energy* **46**, 169–188 (2021).

45. Zhang, X. & Zhang, Y. Environment-friendly and economical scheduling optimization for integrated energy system considering power-to-gas technology and carbon capture power plant. *J. Clean. Prod.* **276**, 123348 (2020).

46. Final Report of Cost Estimates for Thermal Peaking Plant. *Parsons Brinckerhoff New Zealand Ltd.* June 2008.

47. Jeffrey Goldmeer. Power to Gas: Hydrogen for Power Generation. *GE Power.* GEA33861(02/19)

48. Michael J. Reale. New High Efficiency Simple Gas Cycle Gas Turbine – GE's LMS 100. *GE Energy*. GE4222A(06/04)

49. Sokhanvar, K., Karimpour, A. & Pariz, N. Electricity Price Forecasting Using a Clustering Approach. in *2008 IEEE 2nd International Power and Energy Conference* 1302–1305 (2008). doi:10.1109/PECON.2008.4762677.

50. Li, C., Conejo, A. J., Siirola, J. D. & Grossmann, I. E. On representative day selection for capacity expansion planning of power systems under extreme operating conditions. *Int. J. Electr. Power Energy Syst.* **137**, 107697 (2022).

51. Scott, I. J., Carvalho, P. M. S., Botterud, A. & Silva, C. A. Clustering representative days for power systems generation expansion planning: Capturing the effects of variable renewables and energy storage. *Appl. Energy* **253**, 113603 (2019).

52. T. Warren Liao. Clustering of Time Series Data- A Survey. The Journal of Pattern Recognition Society **38**(2005), 1857-1874

53. Dongkuan Xu, & Yingjie Tian. A Comprehensive Survey of Clustering Algorithms. Ann. Data. Sci. (2015) 2(2):165–193

54. Xu R, Wunsch D (2005) Survey of clustering algorithms. IEEE Trans Neural Netw 16:645–678

55. Kaufman, L. & Rousseeuw, P. J. Partitioning Around Medoids (Program PAM). in *Finding Groups in Data: An Introduction to Cluster Analysis* vol. 344 68–125 (In, 1990).

56. SAS Institute Inc. *SAS/STAT(R) 9.2 User's Guide, Second Edition*. (SAS Campus Drive Cary, NC, 2009).

57. Górecki, T. & Łuczak, M. Using derivatives in time series classification. *Data Min Knowl Disc* **26**, 310–331 (2013).

58. Modekurti, S. *et al.* Design, dynamic modeling, and control of a multistage CO2 compression system. *Int. J. Greenh. Gas Con.* **62**, 31–45 (2017).

59. Plócker, U., Knapp, H. & Prausnltz, J. Calculation of high-pressure vapor–liquid equilibria from a corresponding-states correlation with emphasis on asymmetric mixtures. *Ind. Eng. Chem. Process Des. Dev.* **17**, 324–332 (1978)

60. Stoica, P., & Selen, Y. Model-order selection: a review of information criterion rules, *IEEE Signal Processing Magazine* (July): 36–47, doi:10.1109/MSP.2004.1311138

61. Wang, Y., Bhattacharyya, D. & Turton, R. Evaluation of Novel Configurations of Natural Gas Combined Cycle (NGCC) Power Plants for Load-Following Operation using Dynamic Modeling and Optimization. *Energy and Fuels* **34**, 1053–1070 (2020).

62. Wang, Y., Bhattacharyya, D. & Turton, R. Evaluation of Novel Configurations of Natural Gas Combined Cycle (NGCC) Power Plants for Load-Following Operation using Dynamic Modeling and Optimization. *Energy and Fuels* **34**, 1053–1070 (2021).

63. Roberta C., Enrico B. & Lucal D. Z. Techno-Economic Model for Scaling Up of Hydrogen Refueling Stations. *Energies* **2022,**15,7518

64. Bristowe, G. & Smallbone, A. The key techno-economic and manufacturing drivers for reducing the cost of power-to-gas and a hydrogen-enabled energy system. *Hydrogen* **2**, 273–300 (2021)

65. Gas Turbine World (USPS 944760. ISSN 0746-4134)

APPENDIX

APPENDIX I

The output variables generated from aspen model and their units for the development of the reduced order model of the compression train system is represented in the table 1A below.

Table 1A: Output variables extracted from Aspen Model

MODEL		OUTPUT NAME	Units
Output	1	CO_2 Flowrate to Storage	kmol/hr
Output	2	Cooling Duty in Interstage Cooler 1	GJ/hr
Output	3	Cooling Duty in Interstage Cooler 2	GJ/hr
Output	4	Cooling Duty in Interstage Cooler 3	GJ/hr
Output	5	Cooling Duty in Interstage Cooler 4	GJ/hr
Output	6	Cooling Duty in Interstage Cooler 5	GJ/hr
Output	7	Cooling Duty in Interstage Cooler 6	GJ/hr
Output	8	Power Consumption in Compressor 1	kW
Output	9	Power Consumption in Compressor 2	kW
Output	10	Power Consumption in Compressor 3	kW
Output	11	Power Consumption in Compressor 4	kW
Output	12	Power Consumption in Compressor 5	kW
Output	13	Power Consumption in Compressor 6	kW
Output	14	Power Consumption in Compressor 7	kW
Output	15	Power Consumption in Compressor 8	kW

APPENDIX II

The plots for the linear and the nonlinear models developed for the compressor model and the TEG dehydration system model. In order to visually validate the developed ROM for the variables, these plots were generated to observe the closeness of the actual model (aspen model) to the ROM.
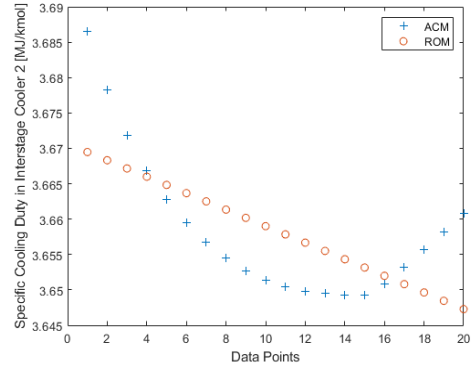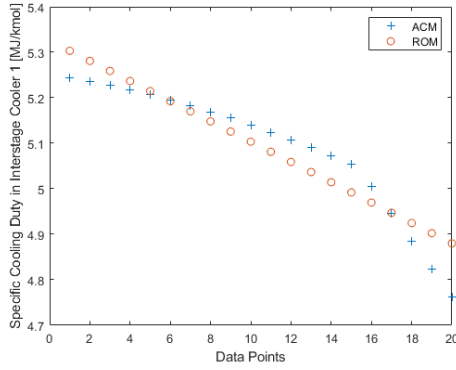

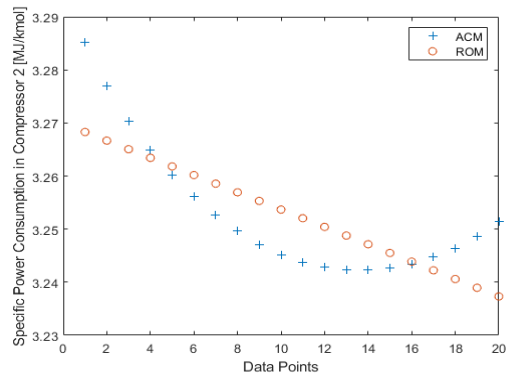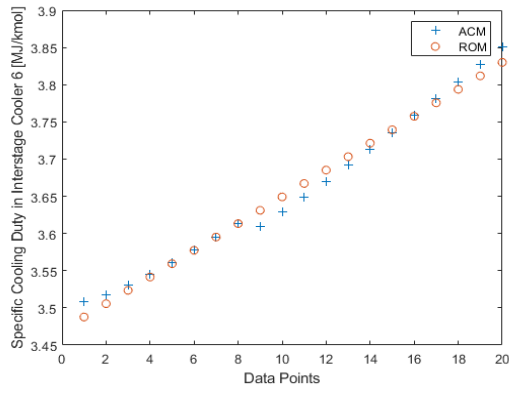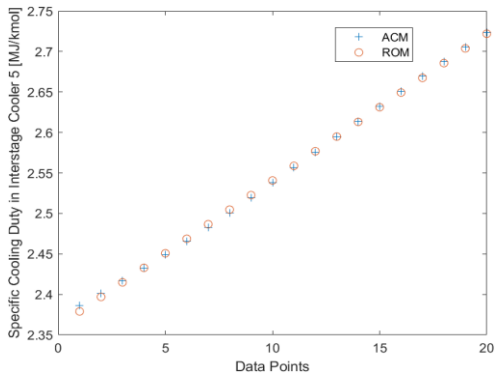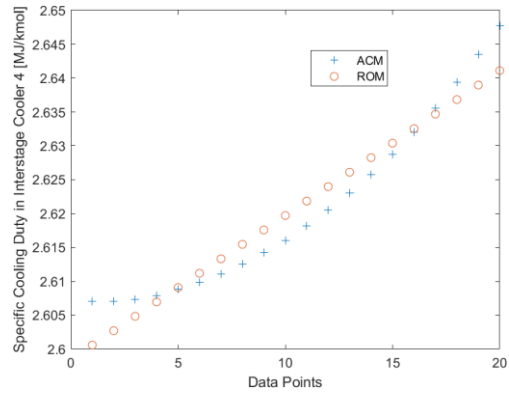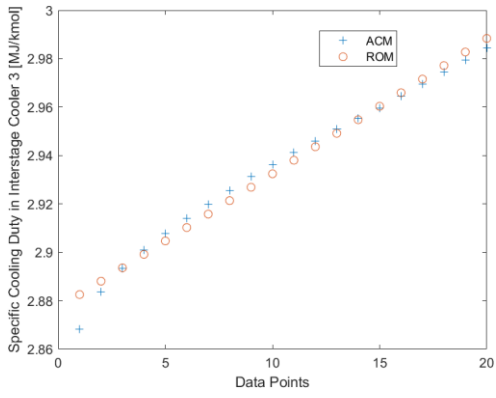**Figure 2A (1-2): Validation plots of the linear output models against the actual model**
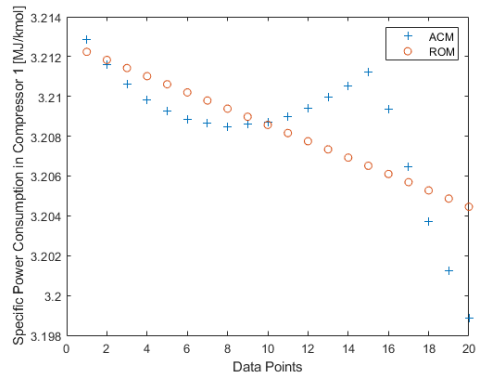
Figure 2A (3-8): Validation plots of the linear output models against the actual model
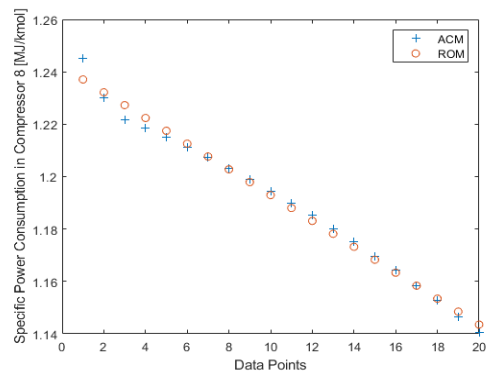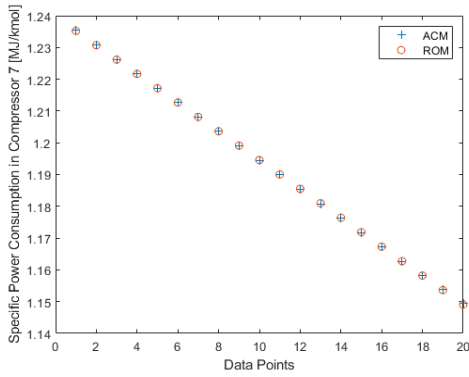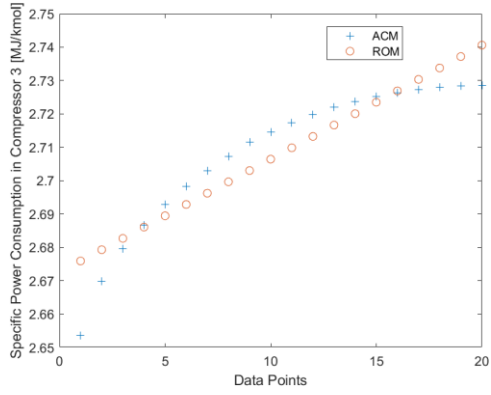
Figure 2A (8-14): Validation plots of the linear output models against the actual model
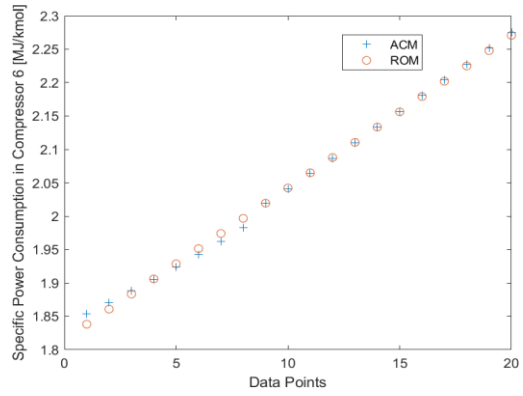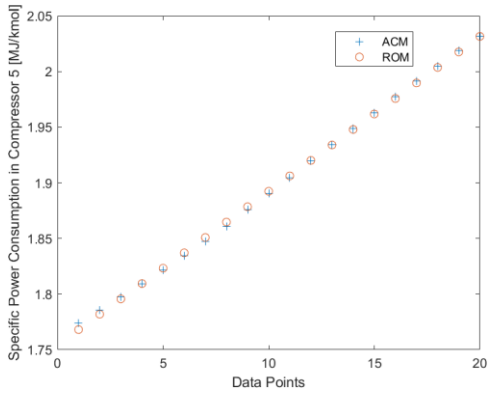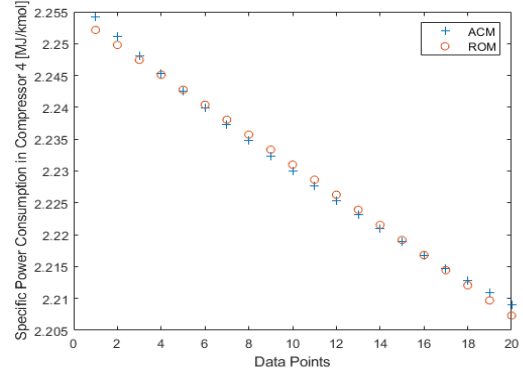
Figure 2B (1-6): Validation plots of the 6 nonlinear output models that didn't conform to linear model against the actual model
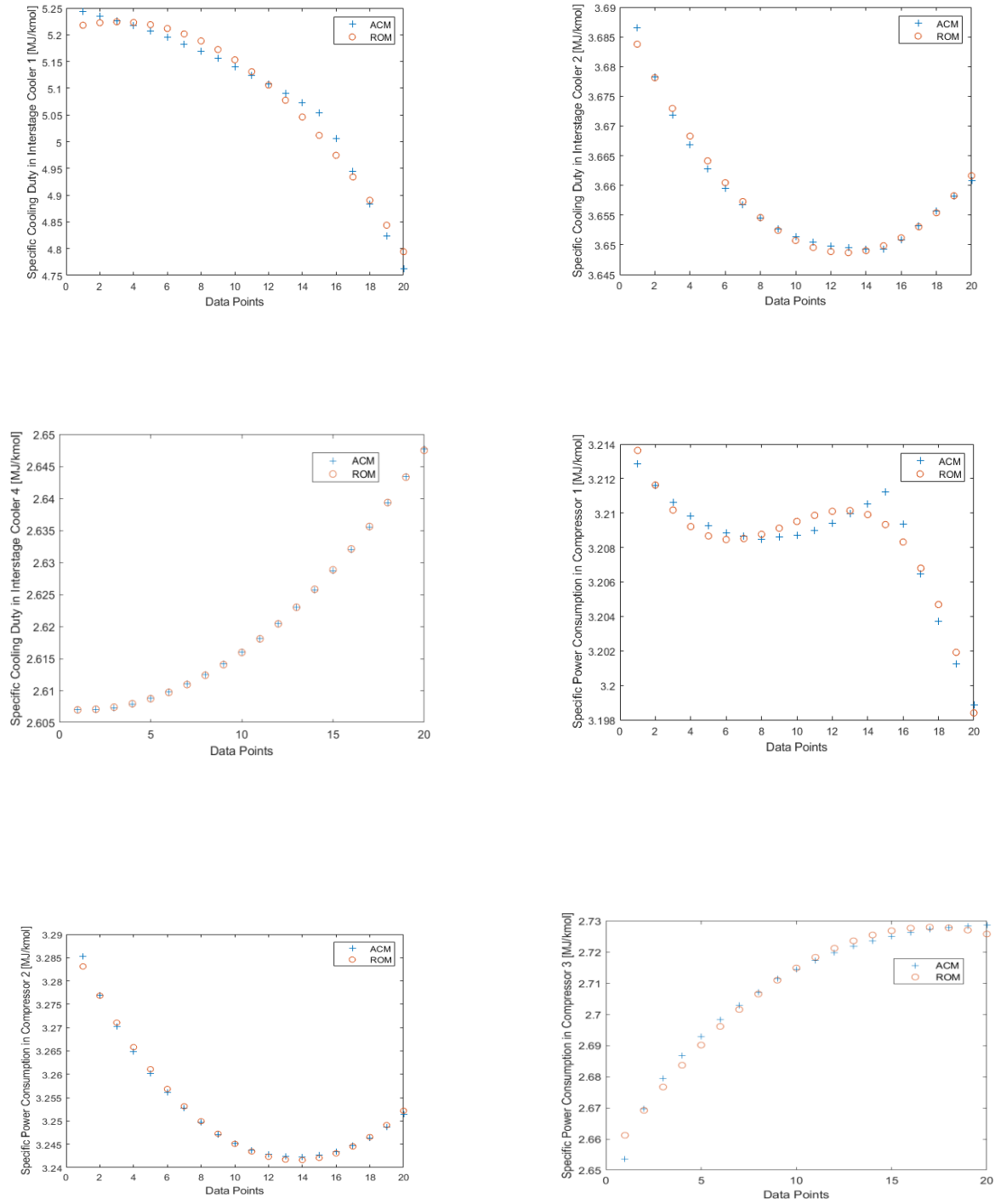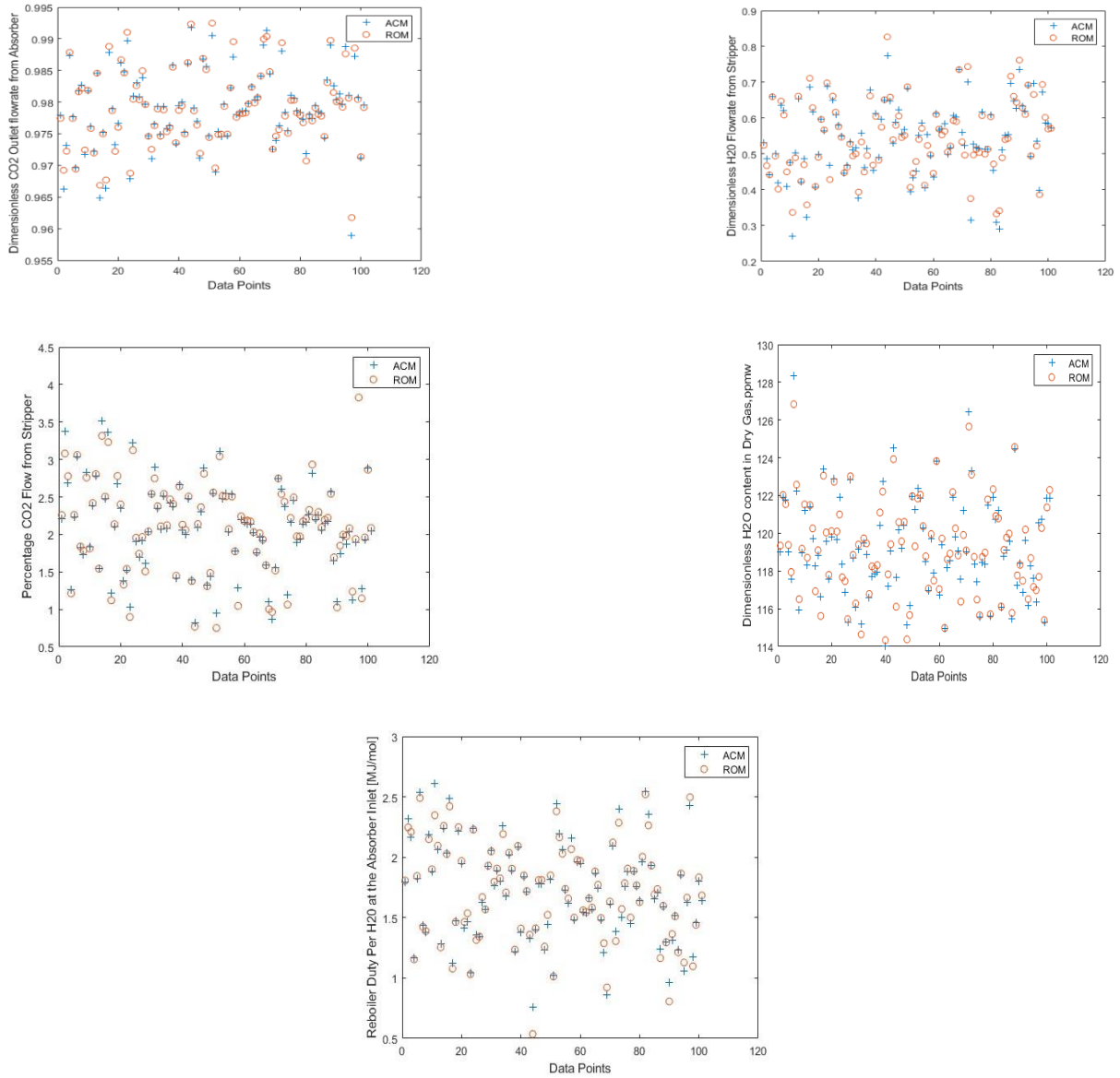
Figure 2C (1-5): Validation plots of the dehydration system linear output models against the actual model
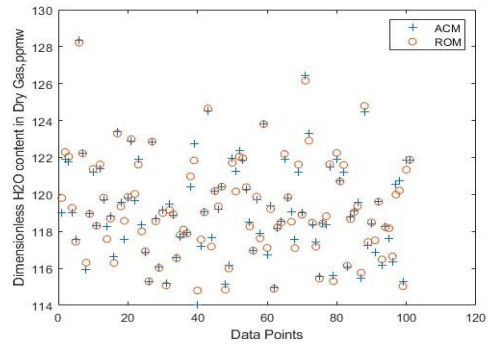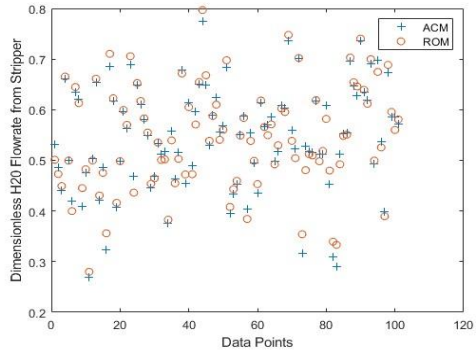
Figure 2C (1-2): Validation plots of the dehydration system nonlinear output models against the actual model

APPENDIX III

A brief description of the process parameters used for hydrogen storage modelling shown in Table 3A.

Table 3A. Process parameters and variables for Hydrogen storage models

	Parameters
C_{p,H_2}	Constant pressure heat capacity of hydrogen (14.33)
z_i	Compressibility factor of hydrogen in compressor i. $z_1 = 1.015$, $z_2 = 1.02$.
$T_{i,in}$	Temperature of hydrogen going into compressor i/storage, where i=1,2 are compressors and i=3 is the storage vessel
η_{comp,H_2}	Electrical efficiency of hydrogen compressors. Set at 0.85.
k	Heat capacity ratio. Set as 1.4.
R	Gas constant
MW_{H_2}	Molecular weight of hydrogen gas
$P_{H_2}^{lb}, P_{H_2}^{ub}$	Lower and upper bounds of hydrogen storage vessel. We let $\left(P_{H_2}^{lb}, P_{H_2}^{ub}\right) = (30,90)$ when considering cylindrical or spherical storage vessels and $\left(P_{H_2}^{lb}, P_{H_2}^{ub}\right) = (40,120)$ when considering cavern storage.
	Variables
V_{H_2}	Design capacity of hydrogen storage vessel (m^3)
$P_{comp,i,t}$	Electrical power consumed by compressor i at time t (MW)
β_t	Compressor ratio
$T_{i,out,t}$	Temperature of hydrogen leaving compressor i at time t (K)

$Q_{cw,i,t}$	Cooling water utility duty of cooler i at time t (MJ/h)
$P_{H_2,t}$	Pressure of hydrogen storage vessel at time t (bar)
$\rho_{H_2,t}$	Density of hydrogen storage at time t (kg/m^3)
$\dfrac{d\rho_{H_2,t}}{dt}$	Time derivative of hydrogen storage density
$\rho_{H_2,int}$	Initial density of hydrogen storage (kg/m^3)
$H_{2,prod,t}$	Hydrogen production rate (kg/h)
$H_{2,inj,t}$	Flow rate of hydrogen injected into NGCC feed (kg/h)

Table 3B. Optimization constraints for NPV optimization of the Integrated NGCC Plant

max	$NPV = P_{A,f}\,(1-tax)\displaystyle\sum_{t\in T} REVENUE_t - CAPEX\left(1 - \dfrac{tax}{n}P_{A,f}\right)$	(A1)
	$P_{A,f} = \dfrac{(1+i)^n - 1}{i(1+i)^n}\cdot\dfrac{1}{(1+i)^n}$	(A2)
$\forall\,t\in T$	$REVENUE_t = LMP_t P_{grid,t} - C_{NG}NG_t - C_{CO_2}CO_{2,released} + C_{H_2}H_{2,credit}$ $- OPEX_{variable} - OPEX_{fixed}$	(A3)
$\forall\,t\in T$	$P_{grid,t} = P_{gross,t} - P_{cons,t}$	(A4)
$\forall\,t\in T$	$cost_{su}[t] = C_{su}\dfrac{1}{1 + e^{-k(d_{sd}[t]-d_{sd}[t-1]-a)}}$	(A5)
NGCC		
$\forall\,t\in T$	$\dot{x}_t = A_{ROM}x_t + B_{ROM}u_t$	(A6)
$\forall\,t\in T$	$y_t = C_{ROM}x_t + D_{ROM}u_t$	(A7)

	PCC	
$\forall\, t \in T$	$\dot{m}_{CO_2,captured,t} = \alpha_{cap,t}\dot{m}_{CO_2,t}$	(A12)
$\forall\, t \in T$	$\alpha_{cap,t} \leq \theta_{des}$	(A13)
$\forall\, t \in T$	$\dot{m}_{CO_2,released,t} = \dot{m}_{CO_2,t} - \dot{m}_{CO_2,captured,t}$	(A14)
$\forall\, t \in T$	$P_{pcc,reboiler,t} = \dot{m}_{CO_2,captured,t} \times Q_{pcc,reboiler} \times \eta_{reboiler}$	(A15)
$\forall\, t \in T$	$P_{pcc,pump,t} = Q_{pcc,pump}\,\dot{m}_{CO_2,captured,t}$	(A16)
$\forall\, t \in T$	$P_{pcc,cooler,t} = Q_{pcc,cooler} \times \dot{m}_{CO_2,captured,t} \times \eta_{cooler}$	(A17)
	CO2 Compression	
$\forall\, i \in [1,14]$ $\forall\, t \in T$	$y_{CO_2-comp,i,t} = a_i + b_i u_{CO_2-comp,t} + c_i u^2_{CO_2-comp,t} + d_i u^3_{CO_2-comp,t}$	(A18)
	Electrolyzer	
$\forall\, t \in T$	$H_{2,prod,t} = Elec_{cap}Elec_{util,t}\eta^{elec}$	(A19)
	H2 Comp	
$\forall\, i \in \{1,2\}$ $\forall\, t \in T$	$P_{comp,i,t} = \left(100 z_i * \dfrac{k}{k-1}\right)\dfrac{H_{2,prod,t}RT_{i,in}}{MW_{H_2}\eta_{comp,H_2}}\left(\beta_t^{\frac{k-1}{k}} - 1\right)$	(A20)
$\forall\, t \in T$	$\beta_t = \sqrt{\dfrac{P_{H_2,t}}{30}}$	(A21)
$\forall\, i \in \{1,2\}$ $\forall\, t \in T$	$T_{i,out,t} = T_{i,in}\left(\dfrac{\beta_t^{\frac{k-1}{k}} - 1}{\eta_{comp,H_2}} + 1\right)$	(A22)
$\forall\, i \in \{1,2,3\}$ $\forall\, t \in T$	$Q_{cw,i,t} = H_{2,prod,t}C_{p,H_2}\left(T_{i,out,t} - T_{i+1,in}\right)$	(A23)
$\forall\, t \in T$	$\dfrac{d\rho_{H_2,t}}{dt} = \dfrac{H_{2,prod,t} - H_{2,inj,t}}{V_{H_2}}$	(A24)

$\forall\, t \in T$	$$\rho_{H_2,t} = \frac{P_{H_2,t} MW_{H_2}}{z_2 R T_{storage}}$$	(A25)
	$\rho_{H_2,int} = \rho_{H_2,final}$	(A26)
$\forall\, t \in T$	$H_{2,prod,t} \cdot H_{2,inj,t} \leq 100$	(A27)

APPENDIX IV

Table 4A. Parameters for Costing of Cylindrical Hydrogen Vessel

Parameter	Horizontal Process Vessels	Vertical Process Vessels
k1	3.5565	3.4974
k2	0.3776	0.4485
k3	0.0905	0.1074
B1	1.49	2.25
B2	1.52	1.82

The result generated and plotted from aspen in the development of the steady state electrolyzer model using aspen plus and aspen custom modeler [42]. The effects of temperature at a fixed pressure and pressure at a fixed temperature are investigated for hydrogen production, efficiency, and power consumption term.
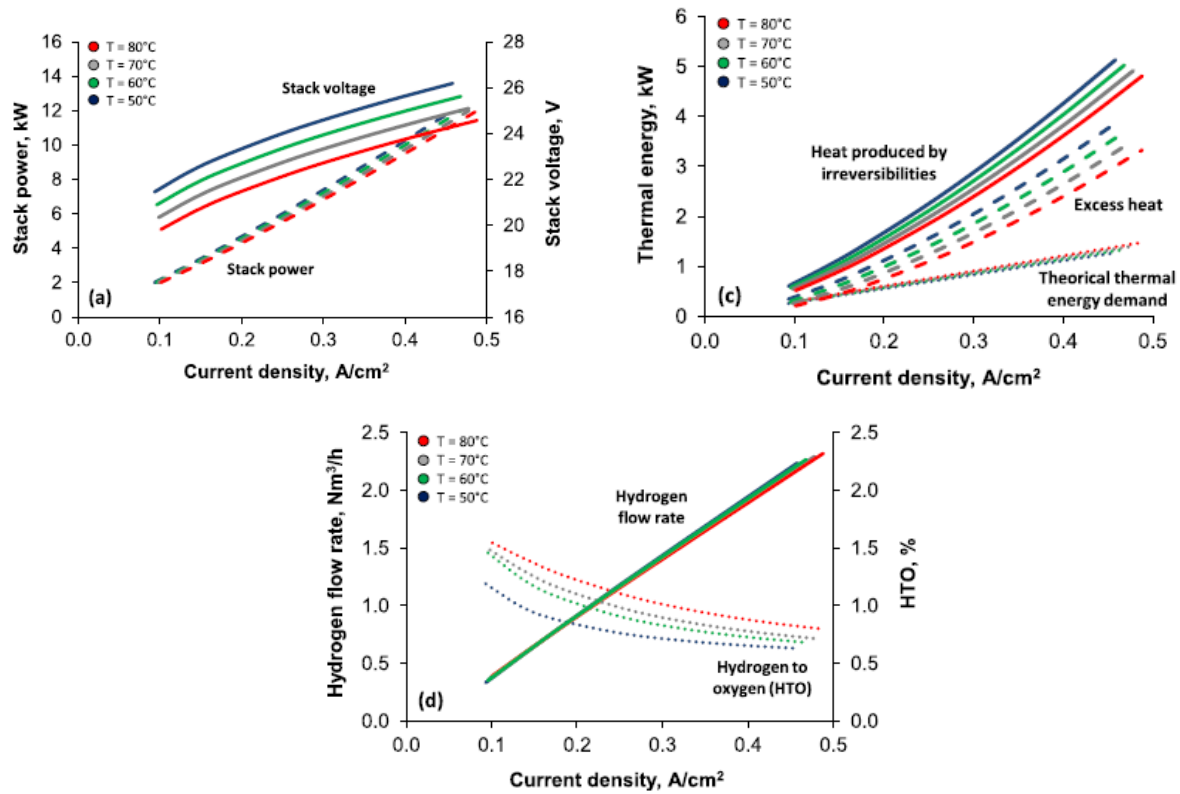

Figure 4A. Effect of temperature on an AEL stack performance at 7 bars: a) Polarization curve and stack power required; b) Heat generated, heat required and excess heat; c) Hydrogen flow rate and hydrogen crossover (HTO).

Figure 4B. Effect of pressure on an AEL stack performance at 75°C: a) Polarization curve and stack power required; b) Heat generated, heat required and excess heat; c) Hydrogen flow rate and hydrogen crossover (HTO).
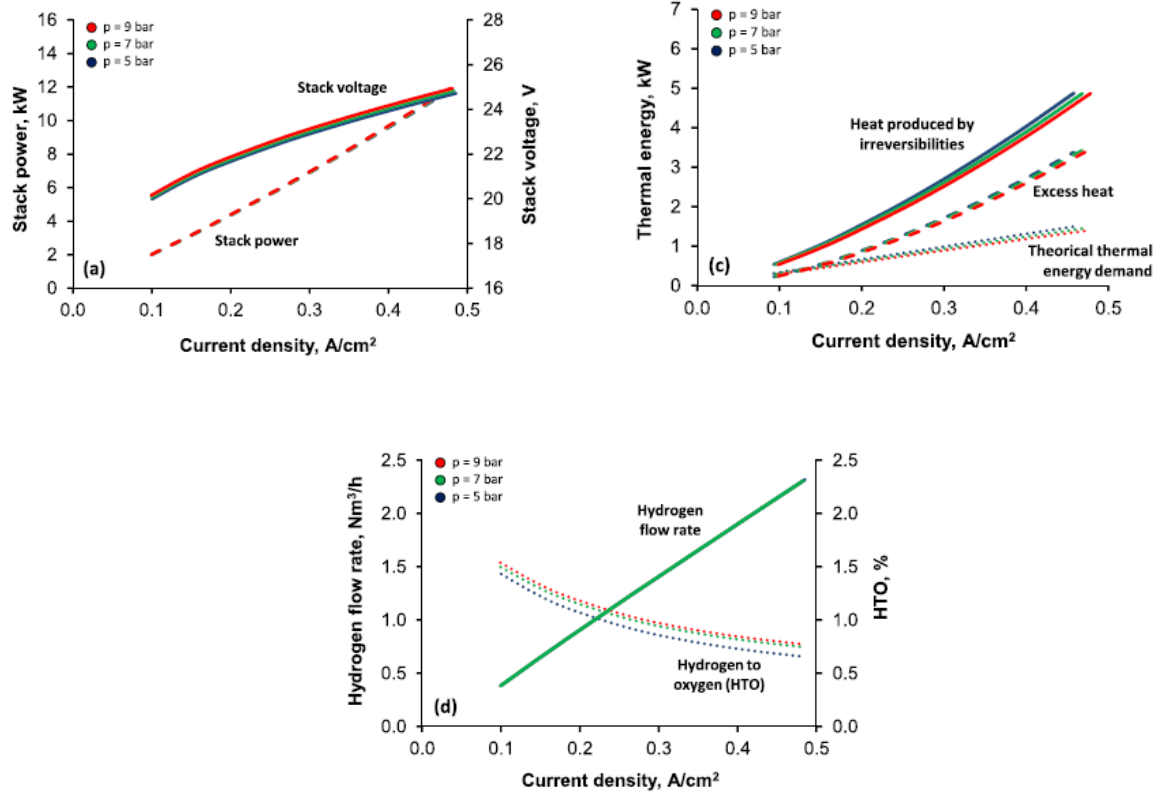
max	$$NPV = P_{A,f} \sum_{t \in T} REVENUE_t - CAPEX$$	(B1)
	$$P_{A,f} = \frac{(1+i)^n - 1}{i(1+i)^n} \cdot \frac{1}{(1+i)^n}$$	(B2)
$\forall\, t \in T$	$$REVENUE_t = LMP_t P_{grid,t} - C_{NG} NG_t - C_{CO_2} CO_{2,released} - OPEX_{variable}$$ $$- OPEX_{fixed}$$	(B3)
$\forall\, t \in T$	$$P_{grid,t} = P_{gross,t} - P_{cons,t}$$	(B4)
Aeroderivative Gas Turbine		
$\forall\, t \in T$	$$Eff_t = 0.2556 + 8e^{-6} P_{output,t} - 1e^{-10} P_{output,t}^2$$	(B6)
$\forall\, t \in T$	$$Eff_t = \frac{Work\ Output(Power\ produced)\ MW_{e,t}}{Heat\ Input\ MW_{th}, t}$$	(B7)
$\forall\, t \in T$	$$Heat\ Input\ (MW_{th}), t = \sum_{f \in H_2, NG} LHV_f * Fuel\ injection\ rate_{f,t}$$	
$\forall\, t \in T$	$$Fuel\ injection\ rate_f \left(\frac{kg}{hr}\right)_t = x_{f,t} \rho_f V_T$$	
$\forall\, t \in T$	$$\sum_{f \in H_2, NG} x_{f,t} = 100$$	
Electrolyzer		
$\forall\, t \in T$	$$EU_t = \frac{Hydrogen\ Producdtion\ rate_t}{Max\ Hydrogen\ Production\ rate}$$	(B8)
$\forall\, t \in T$	$$Hydrogen\ Producdtion\ rate_t \leq Max\ Hydrogen\ Production\ rate$$	(B9)
$\forall\, t \in T$	$$SC_t = 89.54 - 135.17 EU_t + 189.04 EU_t^2 - 80.76 EU_t^3$$	(B10)
$\forall\, t \in T$	$$Actual\ Electrolyzer\ Load_t = SC_t * Hydrogen\ Producdtion\ rate_t$$	(B11)
$\forall\, t \in T$	$$Max\ Electrolyzer\ Load = SC * Max\ Hydrogen\ Producdtion\ rate$$	(B12)
H2 Compressor		

$\forall\, i \in \{1,2\}$ $\forall\, t \in T$	$$P_{comp,i,t} = \left(100 z_i * \frac{k}{k-1}\right) \frac{H_{2,prod,t} R T_{i,in}}{MW_{H_2} \eta_{comp,H_2}} \left(\beta_t^{\frac{k-1}{k}} - 1\right)$$	(B13)
$\forall\, t \in T$	$$\beta_t = \sqrt{\frac{P_{H_2,t}}{30}}$$	(B14)
$\forall\, i \in \{1,2\}$ $\forall\, t \in T$	$$T_{i,out,t} = T_{i,in}\left(\frac{\beta_t^{\frac{k-1}{k}} - 1}{\eta_{comp,H_2}} + 1\right)$$	(B15)
$\forall\, i \in \{1,2,3\}$ $\forall\, t \in T$	$$Q_{cw,i,t} = H_{2,prod,t} C_{p,H_2}\left(T_{i,out,t} - T_{i+1,in}\right)$$	(B16)
$\forall\, t \in T$	$$\frac{d\rho_{H_2,t}}{dt} = \frac{H_{2,prod,t} - H_{2,inj,t}}{V_{H_2}}$$	(B17)
$\forall\, t \in T$	$$\rho_{H_2,t} = \frac{P_{H_2,t} MW_{H_2}}{z_2 R T_{storage}}$$	(B18)
	$$\rho_{H_2,int} = \rho_{H_2,final}$$	(B19)
$\forall\, t \in T$	$$H_{2,prod,t} \cdot H_{2,inj,t} \leq 100$$	(B20)

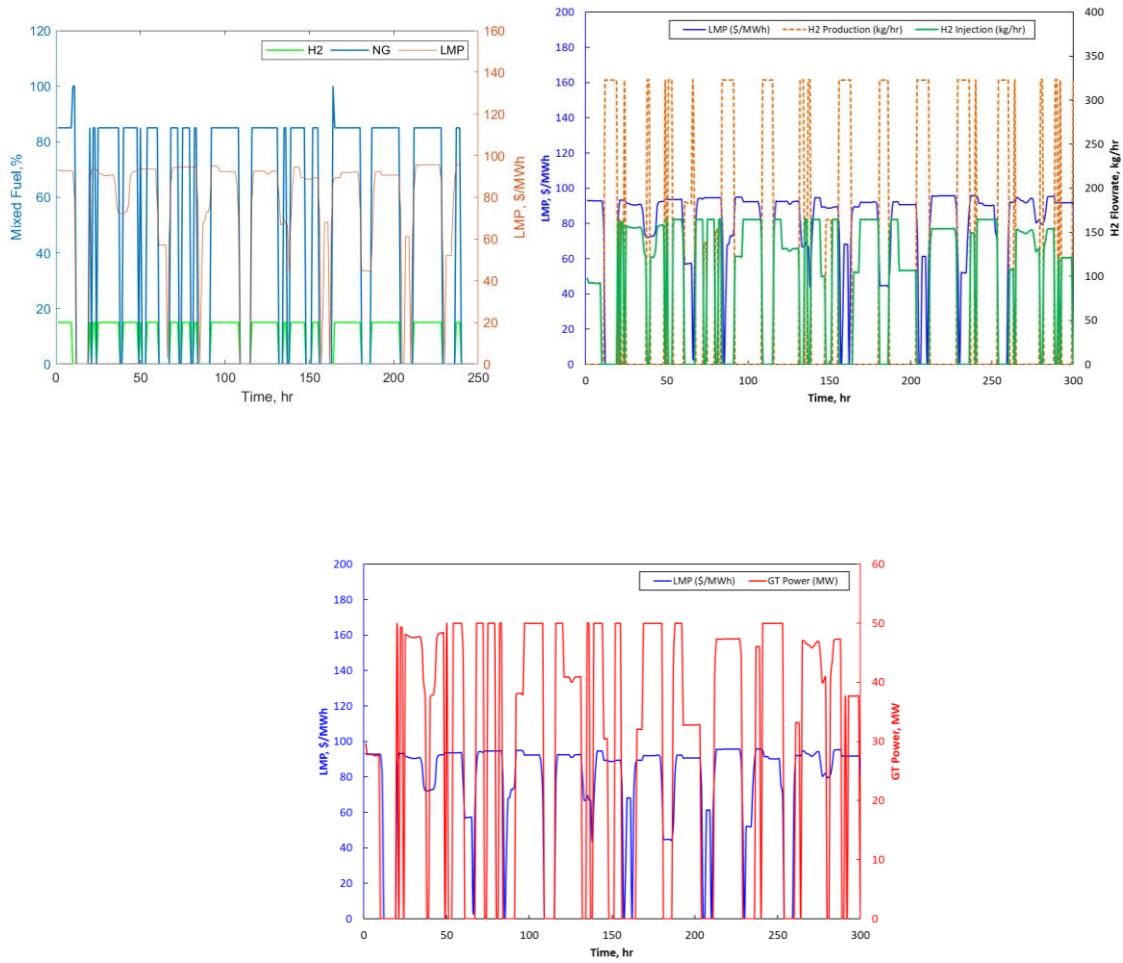**Supplementary Optimization Results**

Figure 4C. Power and hydrogen flowrate profile for 10 days period for Case 3; a. Fuel composition trend b. Hydrogen flowrate trend. c. Gross power GT power trend
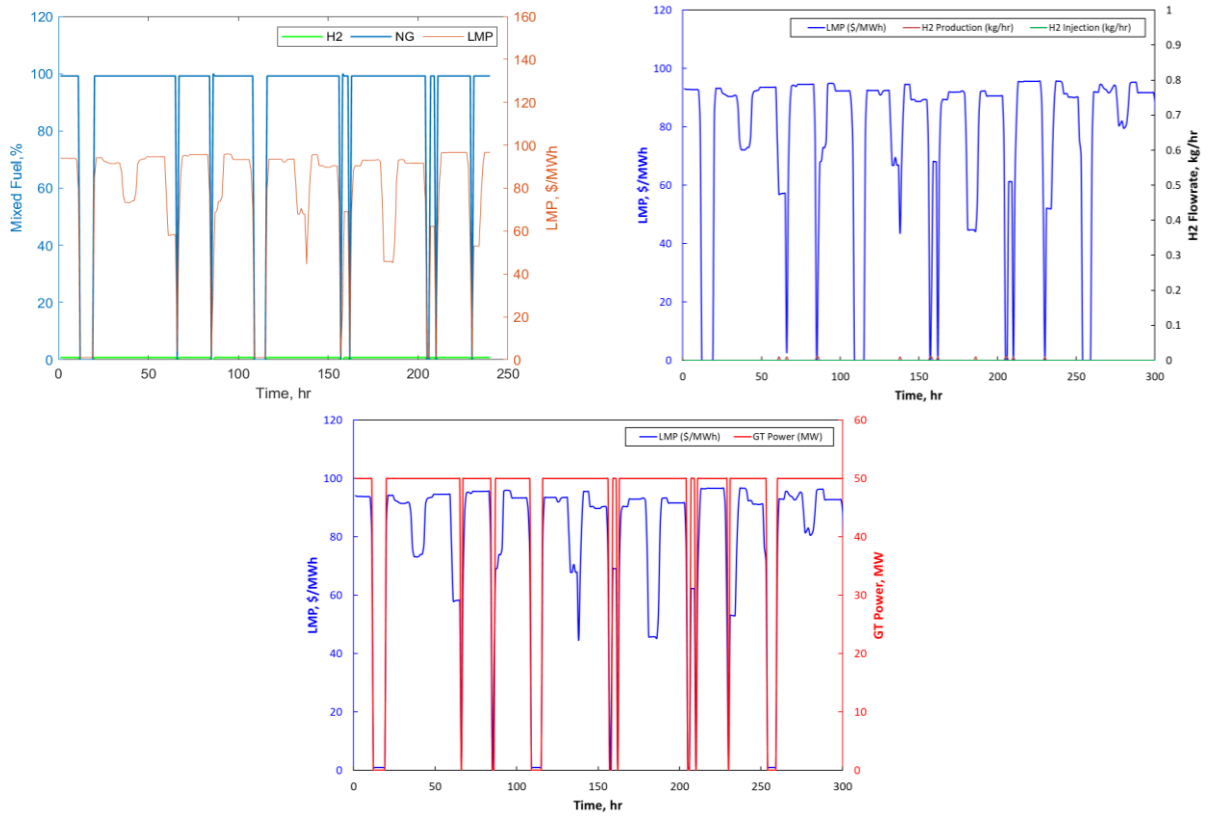
Figure 4D. Power and hydrogen flowrate profile for 10 days period for Case 4; a. Fuel composition trend b. Hydrogen flowrate trend. c. Gross power GT power trend